Detailed efficiency analysis of columns with a different packing quality and confirmation via total pore blocking

Vanderlinden, Kim; Desmet, Gert; Bell, David; Broeckhoven, Ken

Published in:
Journal of Chromatography A

DOI:
10.1016/j.chroma.2018.10.052

Publication date:
2018

Highlights:

-Columns with 4 distinct types of band broadening quality were analyzed

-Retention and peak parking measurements showed identical B-, C_m-, C_s-term dispersion

-Differences could be fully attributed to eddy-dispersion

-Total pore blocking confirmed packing heterogeneity as main difference between columns

Detailed Efficiency Analysis of Columns with a Different Packing Quality and Confirmation via Total Pore Blocking

Kim Vanderlinden[1], Gert Desmet[1], David S. Bell[2], Ken Broeckhoven[1,*]

[1] Vrije Universiteit Brussel, Department of Chemical Engineering, Pleinlaan 2, 1050 Brussels

[2] MilliporeSigma/Supelco, 595 North Harrison Road, Bellefonte, PA 16823, USA

*Corresponding Author: ken.broeckhoven@vub.be, tel.: +32 2 629 32 49

Abstract

We report on a systematic study involving columns with a clearly different efficiency (4 distinct quality groups) obtained by packing the columns that were C_{18} bonded and endcapped with a different carbon loading. Using B-term analysis (via peak parking) and theoretical models to estimate the magnitude of the C_m- and C_s-term contributions, it could be concluded that the difference in efficiency among the groups was entirely due to a difference in eddy dispersion. As such, the columns provided an ideal testing ground to verify how well the total pore blocking (TPB)-method can be used to probe differences in packing heterogeneity. In agreement with earlier literature observations, it turns out the TPB-method is much more sensitive to packing heterogeneities than the eddy dispersion (h_{eddy})-contribution measured under open-pore conditions via B- and C- term subtraction. Typically, differences in h_{eddy} on the order of 0.1-0.5µm translate into a difference on the order of 0.5-2µm in the TPB mode. This confirms the TPB as a powerful technique to make very sensitive measurements of the homogeneity of packed beds.

1. Introduction

In the last 15 years, the column technology in liquid chromatography has witnessed two important evolutions. The first was the introduction of sub-2µm particles at the beginning of this century, readily followed by the introduction of UHPLC instrumentation capable to deliver the high pressures needed to operate these columns at reasonable flow rates [1-5]. The second evolution was the (re-)introduction of core-shell particles, producing reduced plate heights which are 20-30% lower than the traditional h_{min}=2-value which was up till then considered as the performance limit for fully porous particles [5-7]. Originally promoted for their reduced diffusion distance in the porous shell and thus lower mass transfer resistance (C-term), it was later found that the decrease in H was mainly due to a lower longitudinal diffusion (B-term) and a reduced eddy dispersion (A-term). Whereas the underlying reasons for the lower B-term of core-shell particles are well understood, the reason for the strong reduction in A-term is still under debate. One hypothesis is that the smaller A-term contribution is due to the narrower particle size distribution (PSD) of core-shell particles (in turn being a consequence of their production method) [8-12], although this was disputed in other publications [13-15]. In other studies, it was claimed that higher surface roughness results in smaller variations in packing density [11,16] or even lower film mass transfer resistance [13,16]. Supporting the PSD hypothesis however, is that, stimulated by the success of core-shell particles, it was also attempted to produce fully porous particles with a narrower PSD. Doing so, it was indeed found that reduced plate heights between 1.6 and 1.9 (depending on column dimensions) can be obtained for columns packed with fully porous particles [17-19]. Obviously, the PSD cannot be driven to zero as this would lead to regions in the column that are packed into a crystalline configuration, coexisting with randomly packed regions, and this coexistence of poorly and normally permeated regions can lead to a dramatic increase in band broadening.

In the present study, we compared the efficiency of columns packed with C_{18}-derivatized and endcapped silica particles prepared with coating mixtures with increasing theoretical carbon load, i.e., with a composition theoretically leading to a coverage of 2,3,4 or 5 µmol/m^2. For each of the four coverage types, 2 columns were tested, except for the 5µmol/m², for which 3 columns were tested. The different coverage types are referred to in the present study as TC2, TC3, TC4, TC5, using the digit in the abbreviation to represent the theoretical surface coverage in µmol/m^2. Although the packing method for all columns was optimized in the same manner, a systematic and marked difference in overall plate height and eddy-dispersion was observed. To investigate this in detail, a full plate height analysis was made, including testing the columns under total pore blocking (TPB) conditions. This method has been introduced in 2007 [20] and provides indisputably the best measure of packing heterogeneity because, with the particles being completely inaccessible by the analytes, the only remaining dispersion source originates from the heterogeneous network of interstitial flow-through pores. Since its introduction, the TPB method has been applied in a large number of packing heterogeneity studies [16,21-23]. The possible impact of high surface coverage on efficiency has been recently investigated by other authors in chiral chromatography [24-25]. Previous work on the impact of C18 surface coverage on retention and adsorption behavior, as well as on the mass transfer kinetics, can be found in [26-30].

2. Experimental

2.1 Chemicals and columns

HPLC supra-gradient acetonitrile (ACN) and LC-MS grade isopropanol were purchased from Biosolve (Valkenswaard, The Netherlands). Milli-Q water was prepared using a Milli-Q water purification system from Millipore/Merck (MP: Bedford, MA, USA, Merck: Darmstadt, Germany). Decane (≥99%) was purchased from Acros organics (Thermo Fisher Scientific, Waltham, MA, USA). Ammonium acetate (≥97%), acetic acid (≥99.7%), uracil (≥99%), acetophenone (≥99%), propiophenone (≥99%), butyrophenone (≥99%) and potassium iodide (≥99%, KI) were purchased from Sigma-Aldrich (Machelen, Belgium). All columns were Titan C_{18} columns with prototype stationary phase chemistry (see Table 1), with dimensions 3mmx100mm and a particle size of 1.9µm (MilliporeSigma/Supelco, Bellefonte PA, USA). The different stationary phases were subjected to the same proprietary packing optimization procedure to obtain the best packing quality, although, as can be expected, this optimization was not as extensive as for a fully developed and commercialized product. The performance of these columns is thus in no way comparable to the commercial product, for which under similar conditions reduced plate heights below 2 were measured in our lab. The values for C_{18} (primary) and endcapping coverage in Table 1 were obtained by elemental analysis using a Model CHN628 analyzer (LECO, Saint Joseph, Michigan, USA) after each bonding step, where the total coverage is the sum of these two values. The theoretical C_{18} coverage is based on the stoichiometrically available number of C_{18} ligands in the bonding reagent during the primary bonding step, relative to the available surface area of the bare silica stationary phase, i.e., the theoretical maximum bonding assuming all ligands are bound to the surface. The coverage values were determined using the Berendsen coverage calculation [31,32].

2.2 Apparatus

All experiments were conducted on an Agilent 1290 Infinity I UHPLC system (Agilent Technologies, Waldbronn, Germany) equipped with a binary pump, automated sample injector, thermostatted column compartment and a DAD detector with a σ_V = 0.6µL detector cell. Chemstation software (Agilent Technologies) was used for instrument control, data acquisition and analysis. UV signals were recorded at 254nm with a sample rate of 80Hz and the oven temperature was set at 30°C. A stainless steel tubing with an I.D. of 120µm and a length of 28cm was used to connect the injector with the column inlet and a 100µm I.D. PEEK tubing of 22cm was used to connect column outlet and detector. The extra-column peak variance was experimentally measured for all sample components by replacing the column with a zero dead volume (ZDV) union. All presented plate height data have been corrected for the extra-column contributions by subtracting the thus measured variance from the total measured variance when the column was in place. Peak widths were measured at 4.4% height (5σ) as a compromise between accuracy and reproducibility [33]. It was verified that the use of alternative variance measurement methods (peak width at half height or at 4σ; the method of moments) did not alter the observed qualitative differences in observed performance between the different columns.

2.3 Methodology

The sample consisted of three alkylphenones (aceto-, propio- and butyrophenone) and uracil (t_0-marker) dissolved in the same solvent as the mobile phase with a concentration of 100µg/mL and the injection

volume was fixed at 1µL. All experiments (performance, retention, peak parking) were performed in triplicate. For the van Deemter curves, the mobile phase composition was slightly adjusted for each stationary phase (see Table 1) to have the retention factor of propiophenone close to k=7. Columns with the same theoretical carbon load were tested with the same mobile phase composition. The measurements were conducted at flow rates ranging from 0.1 to 1.5mL/min (steps of 0.1mL/min) or until the maximum pump operating pressure was reached (1200bar). For the retention experiments, all measurements were conducted at a flow rate of 0.4mL/min with varying percentage of ACN (25% to 65% in steps of 5% or smaller). In Fig. S1a, the retention factor was fitted according to the Neue-Kuss model to guide the eye [34,35].

$$k = k_w \cdot (1 + S_2 \cdot \varphi)^2 \cdot e^{-\frac{S_1 \cdot \varphi}{1 + S_2 \cdot \varphi}} \quad (1)$$

For the peak parking experiments [36-40], the analyte bands were injected into the column at a flow rate of 0.4mL/min using the same mobile phase conditions as for the van Deemter experiments. When the bands had migrated approximately half way down the column, the flow rate was changed to 0 mL/min in a time frame of 30s and kept at 0.0mL/min for at least 30s to obtain a stable pressure (0 bar) and subsequently increased again in the same 30s time frame up to 0.4ml/min. This gradual decrease and increase in flow rate provided a reproducible decrease and build-up of flow rate and pressure, avoiding experimental variations due to pressure shocks that occur when the flow rate is instantly turned off or on. During the actual peak parking experiments, this procedure was repeated but with extended periods of effective parking time (t_{park}) at zero flow rate (t_{park}=15, 30, 45, 60, 90 and 120 minutes). The observed time-based peak variances (σ_t^2) were converted into distance-based peak variances (σ_x^2) using the measured retained species velocity (u_R). The peak variance $\Delta\sigma_x^2$ acquired by longitudinal diffusion during the effective parking time was calculated by subtracting the peak variance measured for the t_{park}=0s-case. According to Einstein's law of diffusion, the plot of $\Delta\sigma_x^2$ vs. t_{park} should produce a linear relationship with slope $2.D_{eff}$:

$$\Delta\sigma_x^2 = 2 \cdot D_{eff} \cdot t_{park} \quad (2)$$

Total pore blocking (TPB) experiments were conducted according to the method described by Cabooter *et al.* [20]. The columns were first flushed with isopropanol at a flow rate of 0.2mL/min for 1h and then filled with decane at a flow rate of 0.2mL/min for at least 100 column volumes. Finally, the columns were flushed using a 10mM ammonium acetate buffer (pH 3) at a flow rate of 0.4mL/min, injecting 1µL of KI dissolved in the same buffer (100µg/ml) every 5min until t_0-times reached a plateau and column pressures returned to their original values [41]. From these t_0-times the external porosity was calculated using Eq. (3) [20]:

$$\varepsilon = \frac{F \cdot t_0}{V_{geo}} = \frac{V_{int}}{V_{geo}} \quad (3)$$

where F is the flow rate, V_{int} the interstitial pore volume and V_{geo} the geometrical volume of the column (i.e. $\pi \cdot r^2 \cdot L$). Total porosity values ε_T were obtained from the retention time of the t_0-marker for a non-

147 blocked column and are, together with the ε values, reported in Table 1. Internal porosity values were
148 calculated using the relationship between total and external porosity, i.e. $\varepsilon_T=\varepsilon+(1-\varepsilon)\cdot\varepsilon_{int}$.

149

150 ## 3. Results and discussion

151 As shown in Table 1, four degrees of theoretical coverages were considered. These degrees are referred
152 to in the present study as TC2, TC3, TC4, TC5, using the digit in the abbreviation to represent the
153 theoretical surface coverage in $\mu mol/m^2$. For the TC2 columns, a slight tailing was observed for basic
154 analytes (diphenhydramine in 40/60 V%/V% of a 0.1% ammonium acetate buffer/MeOH at 35°C), which
155 increased for even lower primary coverages (results not shown). This can most probably be linked to the
156 incomplete coverage of silanol groups on the surface. It was therefore decided not to investigate lower
157 TC values.

158 As an exemplary illustration of the observed peak width for the different TC's when using neutral
159 compounds (i.e. not affected by residual silanol groups), Fig. 1 shows an overlay and zoom-in of the
160 propiophenone peak in the different chromatograms as measured at a flow rate of 1.2ml/min. As can be
161 noted, each increase in theoretical C_{18} coverage (TC) leads to a systematic and significant loss in
162 efficiency (cf. the fact that the peaks become wider and lower with increasing TC). On the other hand,
163 the effect of the TC on the retention factor is much less pronounced, but still significant (see evolution
164 of k with TC in Fig. 2 further on). These observations are opposite to physical intuition, because an
165 increase in C_{18} coverage is primarily expected to affect the phase ratio and hence the retention
166 properties of the particles, and not as much the band broadening, which is a more mechanical
167 parameter, depending to a large extent on phenomena occurring outside the particles. In below sections
168 this rather unexpected behavior is investigated in a more quantitative way in Sections 3.1-3.2. An in-
169 depth investigation into the cause of this extra band broadening has been carried out as well (Sections
170 3.3-3.5). When interpreting the figures where the observations are plotted versus the theoretical
171 coverage, it should be kept in mind this number might not be linearly related to the true and actual
172 surface coverages. The curve trends in x-direction of the plots should hence not be overinterpreted. For
173 reason of comparison, all figures that use the theoretical coverage as x-axis are repeated in the
174 supplementary information but using the total actual coverage as the x-axis.

175

176 ### *3.1 Surface coverage, retention and porosity values*

177 Table 1 shows the relation between the resulting actual surface coverage and the theoretical carbon
178 load one could expect based on the C_{18} content of the applied coating mixtures. As can be seen from the
179 3rd column in Table 1, the actual primary C_{18} coverage (as measured by elemental analysis) increases in a
180 less than linearly proportional way with the theoretical load based on the composition of the coating
181 mixture. This less than proportional increase is most certainly due to increased steric hindrance effects.
182 The actual C_{18} coverage first increases significantly from TC2 to TC3, then moderately from TC3 to TC4
183 and then levels off (less than 3% difference) for TC5, indicating that further increase in C_{18} coverage is
184 unlikely due to the increased steric hindrance, making the reactive silanol groups no longer accessible.
185 The 4th column of Table 1 shows the extra C_3 coverage obtained in the subsequent endcapping step. As

expected, here an inverse trend with the TC number is observed, as less silanol groups are available after the primary coverage for the highest TC numbers. The result of both coating steps is the total coverage (column nr. 5 in Table 1), calculated here as the sum of the two preceding columns and providing a measure for the number of bonded hydroxyl groups on the surface. As can be noted, the difference in total surface coverage between the different coating recipes is very small (order of 7% increase when going from TC2 to TC5).

To study the high similarity in retention between the different TC-columns in more detail, Fig. 2 shows the retention factor as a function of the theoretical C_{18} surface coverage at 45% ACN, i.e. in the middle of the range covered in Fig. S1a and close to the experimental conditions for the performance measurements discussed further on in this work. It can be observed that the retention factors are to a first approximation independent of the applied TC coating mixtures. The fact that the different TC columns lead to basically the same retention values and dependency on ϕ must obviously be related to the fact that the different TC mixtures lead to very similar total actual surface coverage values (C_{18}+endcap, cf. column nr. 5 in Table 1). This result suggests that the overall ACN-rich partitioning layer that is formed is very similar regardless of the C_{18} density (within the range used in this work). A closer look at Fig. 2 reveals a slight decrease of the retention factors (around 13% for all components at 45 v% ACN) when going from TC2 to TC5. A similar decrease (ranging between 12 and 16%) was found over the entire range (25%-75% ACN) of investigated compositions for all components and column (data not shown). This decrease is more difficult to explain, as it goes against the trend of the increase in C_{18} and the slight increase in total coverage (columns 4&5 in Table 1). At present, we can only speculate this is due to the higher amount of C_{18} molecules present at the higher C_{18} loads, leaving less space for the retained molecules in the stationary phase layer.

Table 1 also shows the values for the external, total and internal porosity obtained for the different TC numbers as respectively derived from the residence time under total pore blocking conditions and from that of an unretained marker (see Experimental). As can be noted, there is no significant difference in external porosity (representative of the packing density) between the different TCs. The total and internal porosity on the other hand slightly decrease with increasing C_{18} coverage, indicating that the increased fraction of long alkyl chains on the stationary phase decreases the accessible space for the probe compound (uracil).

3.2 Band broadening and van Deemter curves

Fig. 3 shows the van Deemter curves (H vs. u_0) for propiophenone (k=7). For each TC number, the average plate height value of the two different columns belonging to each TC number is given. Fig. S2a in the SM (Section 2) shows the van Deemter curves of the individual columns, showing there is little difference between the performance of columns prepared with the same TC number. The only exception are the highest C_{18} coverage columns (TC5) where a stronger variation in column performance was observed between the TC5-1 and TC5-2 column, the latter showing a similar performance as the TC4 columns at high velocity but a slightly higher minimum H. It was therefore decided to test an additional column packed of the TC5 particle batch (TC5-3) which showed similar performance in the high velocity region as the first column (TC5-1), but with a lower minimum H as both other TC5 columns. This broader variation in packing quality and performance for the TC5 compared to TC2-TC4 is in

agreement with the experience that more packing optimization efforts were needed for phase TC5 than for the other phases.

Fig. 3 in fact quantifies the relation between increasing TC number and increasing band broadening already observed in Fig. 1, and now reveals this trend is very systematic and holds for all explored velocities. An exception occurs at the lowest velocities, where the band broadening is nearly exclusively determined by the longitudinal diffusion (B-term), and the difference between the different TC columns vanishes. A fully similar behavior was observed for the more weakly (acetophenone, k ~ 3.3) and more strongly (butyrophenone, k ~ 13.6) retained compounds, as is illustrated in Fig. S3 in the Supplementary material (SM, Section 2).

3.3 B-term dispersion and effective longitudinal diffusion

The relative independence of the different TC curves in the low velocity region of Fig. 3 is confirmed and investigated more in depth in Fig. 4a, showing the results of a series of peak parking measurements by plotting the effective diffusion coefficient D_{eff} as a function of the theoretical C_{18} surface coverage. As is known from theory, D_{eff} relates to the B-term via:

$$B = 2 \cdot D_{eff} \cdot (1+k) \quad (4)$$

As can be noted, there is little or no effect of the theoretical C_{18} surface coverage on D_{eff}, an observation holding for all 3 considered compounds. The difference among columns of the same TC number is maximally of the order of some 3.5% and between different TC numbers the difference is maximally 6.5%. As expected from the theory of longitudinal diffusion [42,43], D_{eff} is the highest for the least retained compound as this is the case where the molecules relatively spend the most time in the mobile phase, where they experience a higher diffusion coefficient than under retained conditions. The overall B-term (proportional to 1+k, see Eq. 4) is however still the highest for the more strongly retained compounds.

3.4 Intra-particle diffusion and eddy dispersion contribution

Using the methodology described in detail in earlier publications [38,43,44], the known value of D_{eff} also allows to estimate the magnitude of the diffusion inside the particles, quantified by the intra-particle diffusion coefficient D_{part}. The methodology to be followed to make this estimate is briefly summarized in the Supplementary Material (SM, Section 3) and also requires the knowledge of k and the total (ε_T) and external porosity (ε). The resulting values are presented in Fig. 4b, showing that the particles prepared with the different TC mixtures all yield very similar D_{part}-values. The typical variation (max $\pm$5% vs. average) is of the same order as the largest variation between two columns with the same TC number.

As a side note, it can be remarked that the two most retained compounds have very similar D_{part}-values, while the least retained compound (acetophenone) has a clearly higher intra-particle diffusion (about 40% higher). The fact that D_{part} is highest for the weakly retained compound and then levels off to a more constant value for the more strongly retained compounds is in agreement with earlier studies of D_{part} [40,45].

The fact that the D_{eff}- and D_{part}-data shown in Fig. 4 are basically the same for the 4 different column types implies the differences in H observed in Fig. 3 cannot be caused by differences in B-term diffusion or the particle zone mass transfer resistance (C_s-term band broadening). Since also the retention factors are very similar, the difference can also not be explained from a difference in mobile zone mass transfer resistance (C_m-term band broadening). To investigate this in more detail, the above contributions were subtracted from the total plate height value using a procedure described in [38,46], leaving only the A-term contribution (for a brief summary of the method, the reader is referred to the SM, Section 3 and refs. [38,46,47]).

The result is shown in Fig. 5a, as a plot of the so-called eddy dispersion contribution (H_{eddy}) versus the u_0-velocity. In this plot, the lowest velocity point has been omitted, as it was recently shown that even the smallest error on the measured B-term value can lead to a huge error on the resulting A-term values at low velocities [39].

Fig. 5a shows that the absolute difference between the eddy dispersion values is basically the same as the difference between the H-curves in Fig. 3, implying that the difference in band broadening observed between the different TC columns is due to a difference in eddy dispersion. Similar results were obtained for acetophenone and butyrophenone (see Fig. S4 in the SM, Section 2).

In anticipation of the analysis in the next Section, some of the data points of Fig. 5a (i.e., the ones corresponding to a number of selected flow rates 0.2, 0.4 and 0.6ml/min) are replotted in Fig. 5b, but now as a function of the theoretical surface coverage TC. This figure again shows the increasing trend of H_{eddy} with the theoretical surface coverage. Again, the TC values provide a good spread of the data point in the graph, but the physical meaning of the x-axis should not be overinterpreted as this is not linearly related to the true and actual C_{18} and total surface coverages, although the trend is very similar when plotted vs. the total surface coverage (see Supplementary Information, Fig. S7).

3.5 Dispersion under total pore blocking conditions and packing heterogeneity

To obtain a better insight in the cause of the difference in eddy dispersion observed in Fig. 5, all columns were also subjected to the total pore blocking method [20,38,41] to make the internal volumes of the particles inaccessible for the sample molecules by filling them with a very apolar solvent (decane). By subsequently measuring the band broadening of a polar compound (KI), using a water buffer as mobile phase, only the band broadening occurring in the void volume of the column, i.e. the flow-through pores between the particles, is measured. This measurement hence directly and exclusively measures the packing disorder. A drawback of the method is that it is restricted to relatively low flow rates (therefore the flow rate was limited to 0.6ml/min in the current experiments) because the resulting higher shear rates result in the leakage of the decane from the particle pores, which in turn completely disturbs the detector signal and eventually leads to the unblocking of the particle mesopores.

Fig. 6a shows, in a dimensionless plot of the normalized peak profile versus the dimensionless time t/t_R, the peak profiles eluting from the column under blocked pore conditions for the four different quality groups at a flow rate of 0.4mL/min. As can be noted, the differences in band broadening under blocked

pore conditions (no C_s- or C_m-term contribution) follow the same order (increasing band broadening with increasing TC-number) as the differences in eddy dispersion observed in the previous section. Translating the 5σ-widths of the recorded peaks into plate height values (H_{TPB}), Fig. 6b reveals a clear increase in H_{TPB} with the theoretical C_{18} load of the particles. The overall picture is very similar to that in Fig. 5b, but the increase in H from TC2 to TC5 is larger, around 75%-85% (vs. 40-50% for the non-blocked columns). The values for TC3 and TC4 are also very similar in agreement with the small difference in H_{eddy} at low velocities found in Fig. 5. Since the only source of dispersion in the H_{TPB}-measurements is the heterogeneity of the interstitial space (there is also a B-term contribution but this is known to be only dependent on the packing density, which is virtually identical in all columns), this qualitative agreement shows that the increased band broadening (Fig. 3) and eddy dispersion (Fig. 5) observed when increasing the theoretical C_{18} load can be fully attributed to an increase of the packing heterogeneity. The fact that the increase in H_{TPB} (order of 80% when comparing the lowest with the highest C_{18} load) is larger than the increase in H_{eddy} (order of some 45%) which is measured under normal retention conditions can be explained by the fact that the band broadening under blocked pore conditions is much more sensitive to disorder than under normal retention conditions, where the mesopores are fully accessible to the analytes, such that the trans-particle diffusion can assist in alleviating the velocity biases. Under TPB conditions this alleviation mechanism is blocked, hence the larger dispersion [23]. The fact that H_{TBP} values shown in Fig. 6b are clearly larger than H_{eddy} is also related to the difference in transverse molecular dispersion across the bed. Once pores are blocked, transverse dispersion is significantly reduced for small molecules because intra-particle diffusivity is zero for non-porous particles [48]. Fig. 6c illustrates the rather good correlation between the values of H_{eddy} and H_{TPB}, where a Pearson correlation coefficient of r=0.81 was found if all points are taken into account and r=0.93 if those of the TC2 columns are discarded.

Whereas the lower efficiency of the columns prepared with the higher TC numbers can now be clearly attributed to a difference in packing heterogeneity, we can at present however only speculate on the cause of this increased heterogeneity. The only observation we can report here is that the poorer packing quality of the higher TC columns is in agreement with the practical observations made during the optimization of the packing process of the different phases, where a more elaborate optimization procedure was required for the higher theoretical C_{18} coverage stationary phases. One hypothesis could be that the particles with the higher TC phases have a different aggregation state of the particles. Due to an increase in hydrophobic attractive forces with TC, the particles are kept more closely together in the packing solvent. Likewise, the increased suppression of free surface silanols at high TC could reduce charge repulsion between the particles. It is thus possible that, with increasing TC, it becomes progressively more difficult to find a suitable packing solvent that allows to obtain an aggregation free slurry, which is needed to obtain well packed columns with I.D.'s of 2.1mm or above [49]. We can however also not rule out that the differences in packing quality are due to a poor particle quality (fines, doublets, triplets, coalesced particles, etc...) or a poor selection of the packing method recipe (nature of slurry and pushing solvents, slurry concentration, packing pressure, constant flow or constant pressure packing, etc...). The relatively low overall performance of the tested columns points in this direction, although it should be noted that all particles were functionalized starting from the same batch of silica particles.

4. Conclusions

Although we currently have no explanation for the observed differences in packing quality between the 4 distinct column groups, the measured differences in column efficiency between the columns obtained with different theoretical C_{18}-coverage could be irrefutably linked to the difference in packing quality. This can be concluded because the retention and peak parking measurements showed identical B-, C_m-, C_s-term dispersion and there was a one-to-one correspondence between the total pore blocking (TPB) band broadening and the calculated eddy-dispersion (h_{eddy}) contribution to the overall band broadening. Typically, differences in (h_{eddy}) on the order of 0.1-0.5μm translate into a difference on the order of 0.5-2μm in the TPB mode. This confirms the TPB as a powerful technique to make very sensitive measurements of the homogeneity of packed beds.

Acknowledgement:
Eddie Jones (MilliporeSigma/Supelco) is acknowledged for his contributions in the preparation of the columns, measurement of column properties and discussion of the obtained results.

5. References

[1] I.S. Lurie, High-performance liquid chromatography of seized drugs at elevated pressure with 1.7 μm hybrid C18 stationary phase columns, J. Chromatogr. A 1100 (2005) 168–175.

[2] D.T.-T. Nguyen, D. Guillarme, S. Rudaz, J.-L. Veuthey, Chromatographic behaviour and comparison of column packed with sub-2 μm stationary phases in liquid chromatography, J. Chromatogr. A 1128 (2006) 105–113.

[3] P.W. Carr, D.R. Stoll, X. Wang, Perspectives on Recent Advances in the Speed of High-Performance Liquid Chromatography, Anal. Chem. 83 (2011) 1890-1900.

[4] A. de Villiers, F. Lestremau, R. Szucs, S. Gélébart, F. David, P. Sandra, Evaluation of ultra-performance liquid chromatography: Part I. Possibilities and limitations, J. Chromatogr. A 1127 (2006) 60-69.

[5] Y. Zhang, X. Wang, P. Mukherjee, P. Petersson, Critical comparison of performances of superficially porous particles and sub-2μm particles under optimized ultra-high pressure conditions, J. Chromatogr. A 1216 (2009) 4597-4605.

[6] S. Fekete, E. Oláh, J. Fekete, Fast liquid chromatography: the domination of core–shell and very fine particles, J. Chromatogr. A 1228 (2012) 57–71.

[7] G. Guiochon, F. Gritti, Shell particles, trials, tribulations and triumphs, J. Chromatogr. A 1218 (2011) 1915–1938.

[8] D. Cabooter, A. Fanigliulo, G. Bellazzi, B. Allieri, A. Rottigni, G. Desmet, Relationship between the particle size distribution of commercial fully porous and superficially porous high-performance liquid chromatography column packings and their chromatographic performance, J. Chromatogr. A 1217 (2010) 7074-7081.

[9] D. Cabooter, J. Billen, H. Terryn, F. Lynen, P. Sandra, G. Desmet, Kinetic plot and particle size distribution analysis to discuss the performance limits of sub-2 µm and supra-2 µm particle columns, J. Chromatogr. A 1204 (2008) 1-10.

[10] D. Cabooter, J. Billen, H. Terryn, F. Lynen, P. Sandra, G. Desmet, Detailed characterisation of the flow resistance of commercial sub-2 µm reversed-phase columns, J. Chromatogr. A 1178 (2008) 108-117.

[11] R. Hayes, A. Ahmed, T. Edge, H. Zhang, Core–shell particles: Preparation, fundamentals and applications in high performance liquid chromatography, J. Chromatogr. A, 1357 (2014) 36-52.

[12] K. Horváth, D. Lukács, A. Sepsey, A. Felinger, Effect of particle size distribution on the separation efficiency in liquid chromatography, J. Chromatogr. A 1361 (2014) 203-208.

[13] F. Gritti, G. Guiochon, Comparative study of the performance of columns packed with several new fine silica particles: Would the external roughness of the particles affect column properties, J. Chromatogr. A 1166 (2007) 30-46.

[14] A. Liekens, J. Billen, R. Sherant, H. Ritchie, J. Denayer, G. Desmet, High performance liquid chromatography column packings with deliberately broadened particle size distribution: Relation between column performance and packing structure, J. Chromatogr. A 1218 (2011) 6654-6662.

[15] A. Daneyko, A. Höltzel, S. Khirevich, U. Tallarek, Influence of the particle size distribution on hydraulic permeability and Eddy dispersion in bulk packings, Anal. Chem. 83 (2011) 3903-3910.

[16] F. Gritti, I. Leonardis, J. Abia, G. Guiochon, Physical properties and structure of fine core-shell particles used as packing materials for chromatography: Relationships between particle characteristics and column performance, J. Chromatogr. A 1217 (2010) 3819-1843.

[17] O.H. Ismail, M. Catani, L. Pasti, A. Cavazzini, A. Ciogli, C. Villani, D. Kotoni, F. Gasparrini, D.S. Bell, Experimental evidence of the kinetic performance achievable with columns packed with new 1.9 µm fully porous particles of narrow particle size distribution, J. Chromatogr. A 1454 (2016) 86-92.

[18] M. Catani, O.H. Ismail, A. Cavazzini, A. Ciogli, C. Villani, L. Pasti, C. Bergantin, D. Cabooter, G. Desmet, F. Gasparrini, D.S. Bell, Rationale behind the optimum efficiency of columns packed with new 1.9 µm fully porous particles of narrow particle size distribution, J. Chromatogr. A 1454 (2016) 78-85.

[19] R. Henry, Impact of Particle Size Distribution on HPLC Column Performance, LCGC N. Am. 32 (2014) 12–19.

[20] D. Cabooter, F. Lynen, P. Sandra, G. Desmet, Total pore blocking as an alternative method for the on-column determination of the external porosity of packed and monolithic reversed-phase columns, J. Chromatogr. A. 1157 (2007) 131–141.

[21] F. Gritti, G. Guiochon, Mass transfer mechanism in liquid chromatography columns packed with shell particles: Would there be an optimum shell structure? J. Chromatogr. A 1217 (2010) 8167-8180.

[22] F. Gritti, G. Guiochon, Impact of retention on trans-column velocity biases in packed columns, AlChe J. 56 (2010) 1495-1509.

[23] F. Gritti, G. Guiochon, New insights on mass transfer kinetics in chromatography, AIChE journal, 57 (2011) 333-345.

[24] O.H. Ismail, L. Pasti, A. Ciogli, C. Villani, J. Kocergin, S. Anderson, F. Gasparrini, A. Cavazzini, M. Catani, Pirkle-type chiral stationary phase on core-shell and fully porous particles: Are superficially porous particles always the better choice toward ultrafast high-performance enantioseparations?, J. Chromatogr. A, 1466 (2016) 96-104.

[25] M. Catani, O.H. Ismail, F. Gasparrini, M. Antonelli, L. Pasti, N. Marchetti, S. felletti, A. Cavazzini, Recent advancements and future directions of superficially porous chiral stationary phases for ultra-fast high-performance enantioseparations, Analyst, 142 (2017) 555-566.

[26] B. Buszewski, Sz. Bocian, A. Felinger, Excess isotherms as a new way for characterization of the columns for reversed-phase liquid chromatography, J. of Chromatogr. A 1191 (2008) 72-77.

[27] S. Bocian, P. Vajda, A. Felinger, B. Buszewski, Excess Adsorption of Commonly Used Organic Solvents from Water on Nonend-Capped C18-Bonded Phases in Reversed-Phase Liquid Chromatography, Anal. Chem. 81 (2009) 6334-6346.

[28] F. Gritti, G. Guiochon, Adsorption mechanism in reversed-phase liquid chromatography - Effect of the surface coverage of a monomeric C-18-silica stationary phase, J. Chromatogr. A 1115 (2006) 142-163.

[29] F. Gritti, G. Guiochon, Effect of the density of the C-18 surface coverage on the adsorption mechanism of a cationic compound and on the silanol activity of the stationary phase in reversed phase liquid chromatography, J. Chromatogr. A 1132 (2006) 51-66.

[30] F. Gritti, G. Guiochon, Effect of the surface coverage of C-18-bonded silica particles on the obstructive factor and intraparticle diffusion mechanism, Chem. Eng. Sci. 61 (2006) 7636-7650.

[31] G.E. Berendsen, L. de Galan, Role of the chain length of chemically bonded phases and the retention mechanism in reversed-phase liquid chromatography, J. Chromatogr. 196 (1980) 21.

[32] B. Buszewski, S. Bocian, G. Rychlicki, M. Matyska, J. Pesek, Determination of accessible silanols groups on silica gel surfaces using microcalorimetric measurements, J. Chromatogr. 1232 (2012) 43-46.

[33] Y. Vanderheyden, K. Broeckhoven, G. Desmet, Comparison and optimization of different peak integration methods to determine the variance of unretained and extra-column peaks, J. Chromatogr. A. 1364 (2014) 140–150.

[34] U.D. Neue, H.-J. Kuss, Improved reversed-phase gradient retention modeling, J. Chromatogr. A. 1217 (2010) 3794-3803.

[35] E. Tyteca, A. Périat, S. Rudaz, G. Desmet, D. Guillarme, Retention modeling and method development in hydrophilic interaction chromatography, J. Chromatogr. A 1337 (2014) 116-127.

[36] J.H. Knox, Band dispersion in chromatography – a new view of A-term dispersion, 831 (1999) 3–15.

[37] K. Broeckhoven, D. Cabooter, F. Lynen, P. Sandra, G. Desmet, Errors involved in the existing B-term expressions for the longitudinal diffusion in fully porous chromatographic media: Part II: Experimental data in packed columns and surface diffusion measurements, J. Chromatogr. A. 1188 (2008) 189-198.

[38] A. A. Sanz, K. Broeckhoven, G. Desmet, Methods for the experimental characterization and analysis of the efficiency and speed of chromatographic columns: A step-by-step tutorial, Anal. Chimica Acta, 894 (2015) 20-34.

[39] H. Song, D. Sadriaj, G. Desmet, D. Cabooter, Methodologies to determine b-term coefficients revisited, J. Chromatogr. A 1532 (2018) 124–135.

[40] H. Song, G. Desmet, D. Cabooter, Assessment of intra-particle diffusion in hydrophilic interaction liquid chromatography and reversed-phase liquid chromatography under conditions of identical packing structure, J. Chromatogr. A 1523 (2017) 204–214.

[41] A. Liekens, D. Cabooter, J. Denayer, G. Desmet, A study of the parameters affecting the accuracy of the total pore blocking method, J. Chromatogr. A. 1217 (2010) 6754–6761.

[42] G. Desmet, K. Broeckhoven, J. De Smet, S. Deridder, G. V Baron, P. Gzil, Errors involved in the existing B-term expressions for the longitudinal diffusion in fully porous chromatographic media Part I: computational data in ordered pillar arrays and effective medium theory, J. Chromatogr. A. 1188 (2008) 171–188.

[43] S. Deridder, G. Desmet, Effective medium theory expressions for the effective diffusion in chromatographic beds filled with porous, non-porous and porous-shell particles and cylinders. Part II: Numerical verification and quantitative effect of solid core on expected B-term band, J. Chromatogr. A. 1218 (2011) 46–56.

[44] G. Desmet, S. Deridder, Effective medium theory expressions for the effective diffusion in chromatographic beds filled with porous, non-porous and porous-shell particles and cylinders. Part I: Theory, J. Chromatogr. A. 1218 (2011) 32–45.

[45] A. Liekens, J. Denayer, G. Desmet, Experimental investigation of the difference in B-term dominated band broadening between fully porous and porous-shell particles for liquid chromatography using the Effective Medium Theory J. Chromatogr. A. 1218 (2011) 4406– 4416.

[46] G. Desmet, K. Broeckhoven, Equivalence of the different Cm- and Cs-term expressions used in liquid chromatography and a geometrical model uniting them, Anal. Chem. 80 (2008) 8076–8088.

[47] S. Deridder, G. Desmet, New insights in the velocity dependency of the external mass transfer coefficient in 2D and 3D porous media for liquid chromatography, J. Chromatogr. A. 1227 (2012) 194–202.

[48] F. Gritti, G. Guiochon, Perspectives on the Evolution of the Column Efficiency in Liquid Chromatography, Anal. Chem. 85, (2013) 3017-3035.

[49] M.F. Wahab, D.C. Patel, R.M. Wimalasinghe, D.W. Armstrong, Fundamental and Practical Insights on the Packing of Modern High-Efficiency Analytical and Capillary Columns, Anal. Chem 89 (2017) 8177-8191.

Figure captions

Figure 1: Overlay of the chromatogram peaks for propiophenone (k=7) obtained for the different theoretical coverage cases (TC) at the same linear velocity (u_0). The curves were normalized to surface area and aligned according to their first order moment to highlight the differences in peak width. For each stationary phase, a chromatogram obtained on the first column is presented in the figure. The reported N values are those obtained using the 5σ-method.

Figure 2: Retention factor vs. theoretical C_{18} surface coverage for the different investigated columns at a concentration of 45% volume fraction of acetonitrile for acetophenone (diamonds), propiophenone (squares) and butyrophenone (triangles). Most of the data points (2 per TC, except for TC5 where there are 3 data points) per tested column overlap and are therefore invisible.

Figure 3: Plot of plate height vs. linear velocity for the different theoretical surface coverages for propiophenone as sample compound (k=7); each data set presents the average of two columns with the same stationary phase (or three for TC5). Fit curves according to the van Deemter equation to guide the eye. Symbols: TC2 (squares), TC3 (triangles), TC4 (diamonds), TC5 (circles).

Figure 4: (a) Effective diffusion coefficient D_{eff} and **(b)** intra-particle diffusion coefficient D_{part} for the different theoretical C_{18} coverages; symbols: acetophenone (diamonds), propiophenone (squares) and butyrophenone (triangles). Some of the data points (2 per TC, except for TC5 where there are 3 data points) per tested column overlap and are therefore invisible.

Figure 5: (a) Plot of the eddy dispersion contribution vs. velocity to the overall H for the different surface coverages, fit curves to guide the eye; **(b)** Eddy dispersion contribution as a function of theoretical surface coverage for 0.2 ml/min (triangles), 0.4ml/min (diamonds) and 0.6ml/min (circles). Sample compound propiophenone for both figures.

Figure 6: (a) Plot of the normalized peak profiles recorded under blocked pore conditions versus the dimensionless time t/t_R for the 4 different column types (flow rate = 0.4mL/min). The peak heights (mAu) were normalized by their peak area (mAu·min); **(b)** Plate height measured in a blocked column as a function of theoretical surface coverage for 0.2 ml/min (triangles), 0.4ml/min (diamonds) and 0.6ml/min (circles). **(c)** Plot of plate height measured in a blocked column H_{TPB} vs. the eddy dispersion contribution H_{eddy} for 0.2ml/min (triangles), 0.4ml/min (diamonds) and 0.6ml/min (circles). Linear fit (dotted line) to guide the eye.

Figure 1:

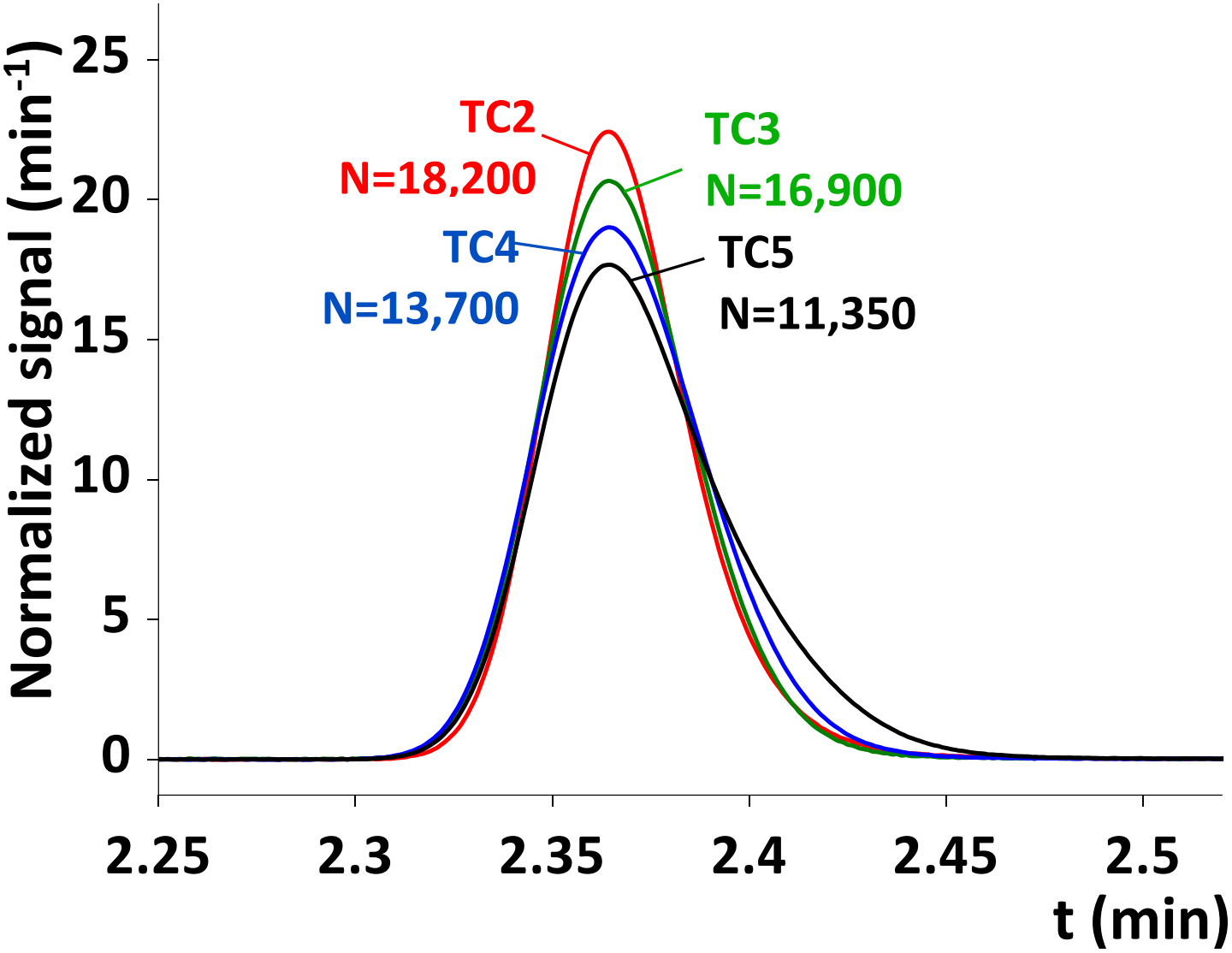
Normalized signal (min-1)
25
20
15
10
5
0
TC2
N=18,200
TC3
N=16,900
TC4
N=13,700
TC5
N=11,350
2.25
2.3
2.35
2.4
2.45
2.5
t (min)

Figure 2:

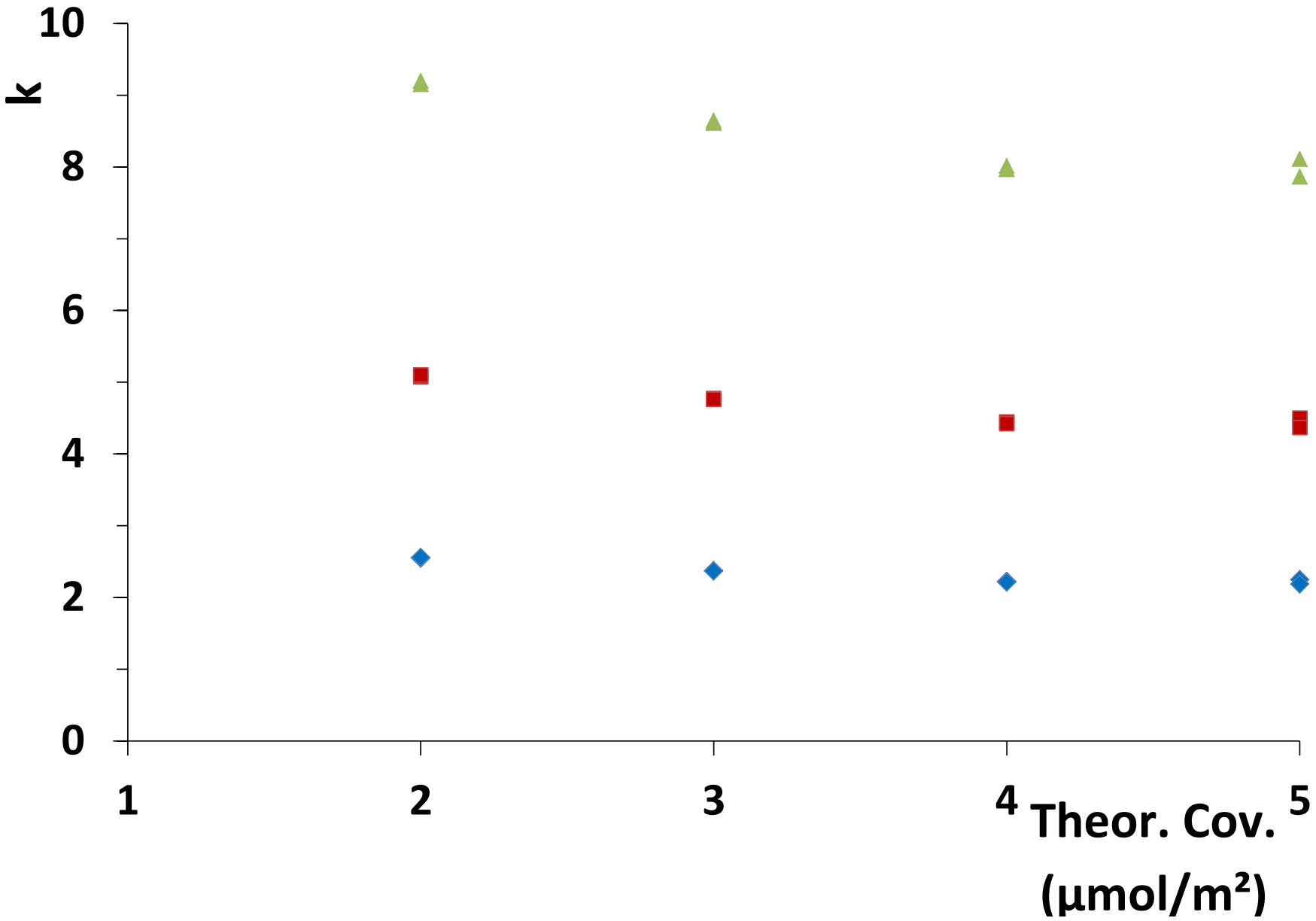

Figure 3:

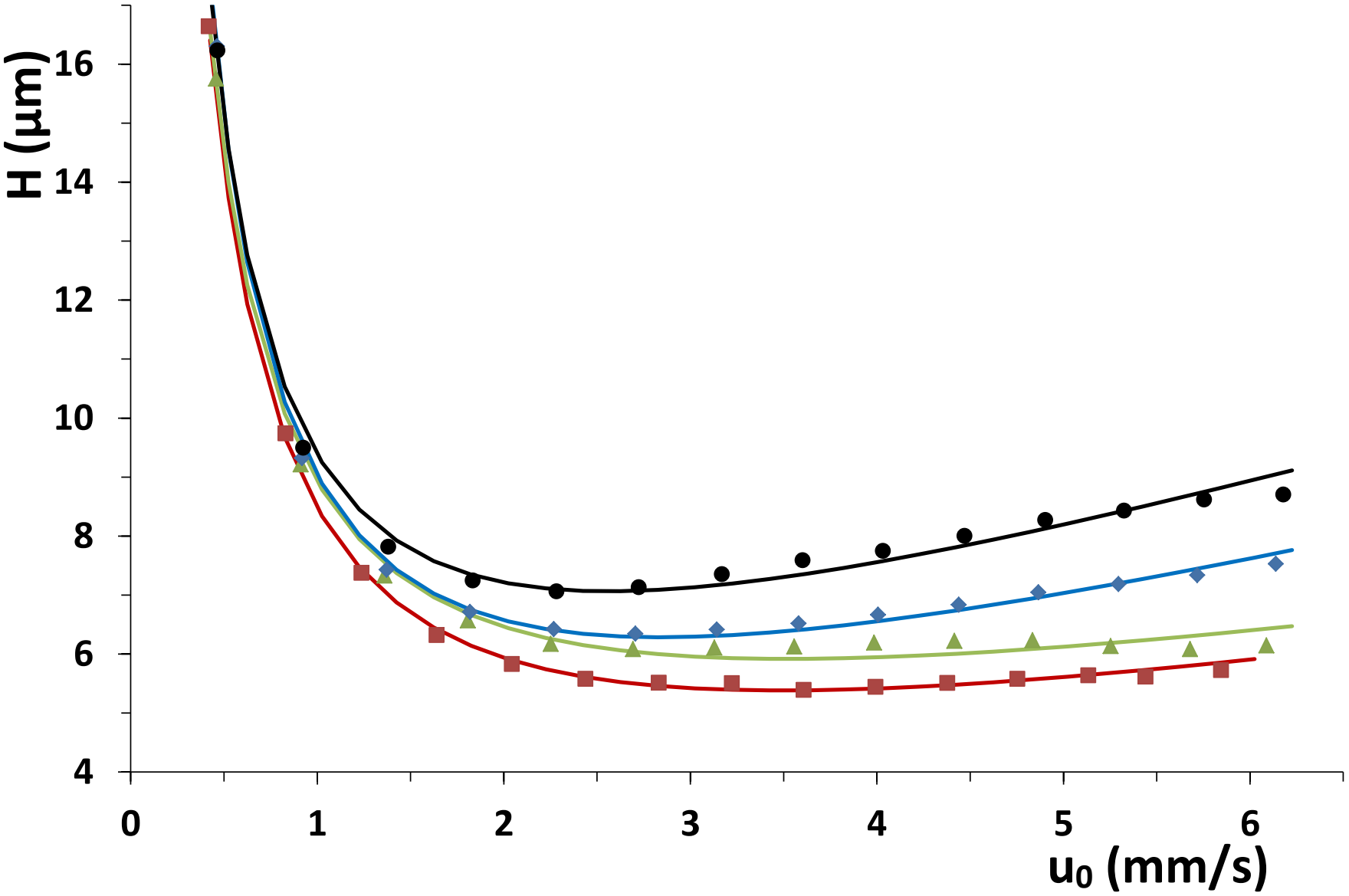

Figure 4:

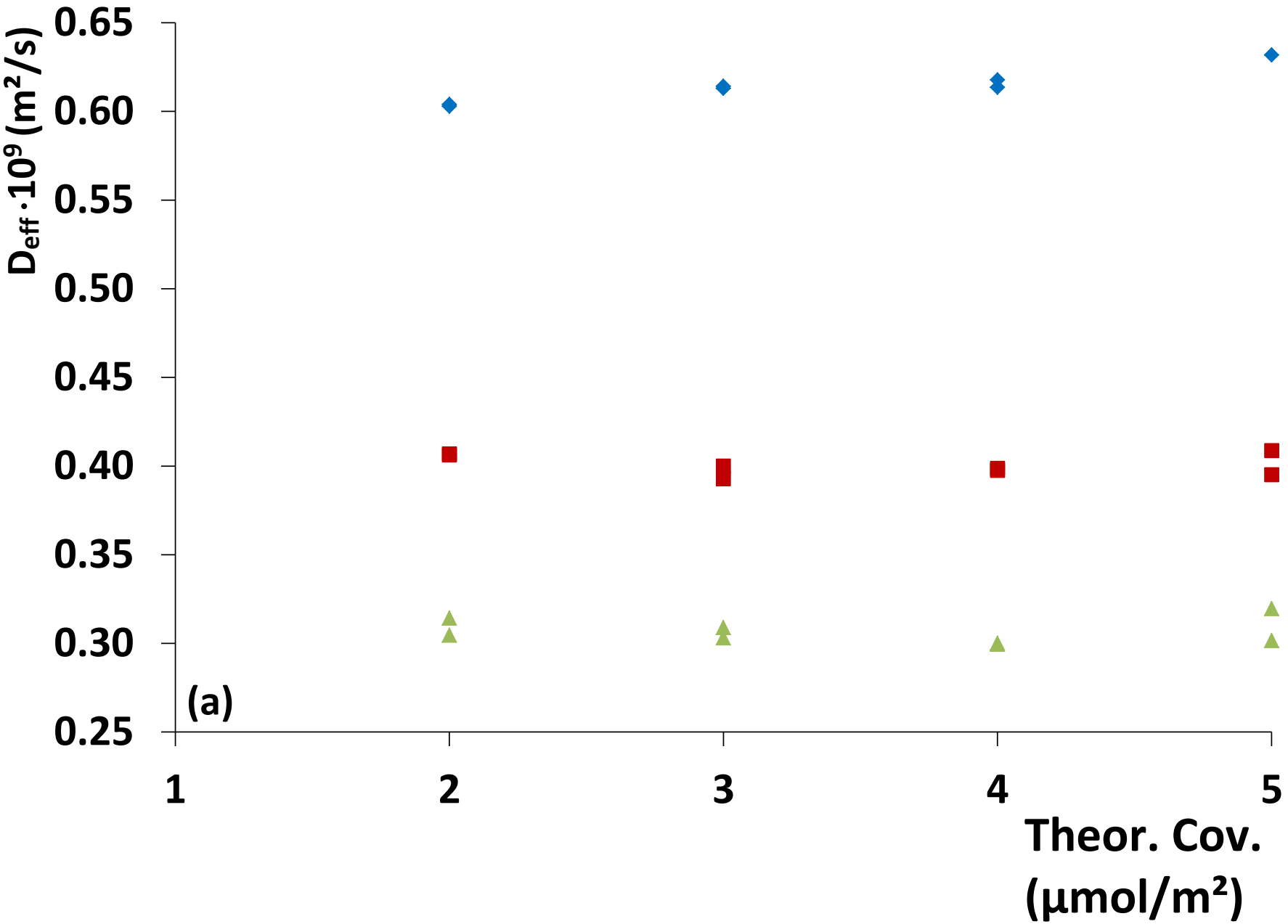
0.65
0.60
0.55
0.50
0.45
0.40
0.35
0.30
0.25
$D_{eff} \cdot 10^9$ (m^2/s)
(a)
1
2
3
4
5
Theor. Cov.
(µmol/m²)

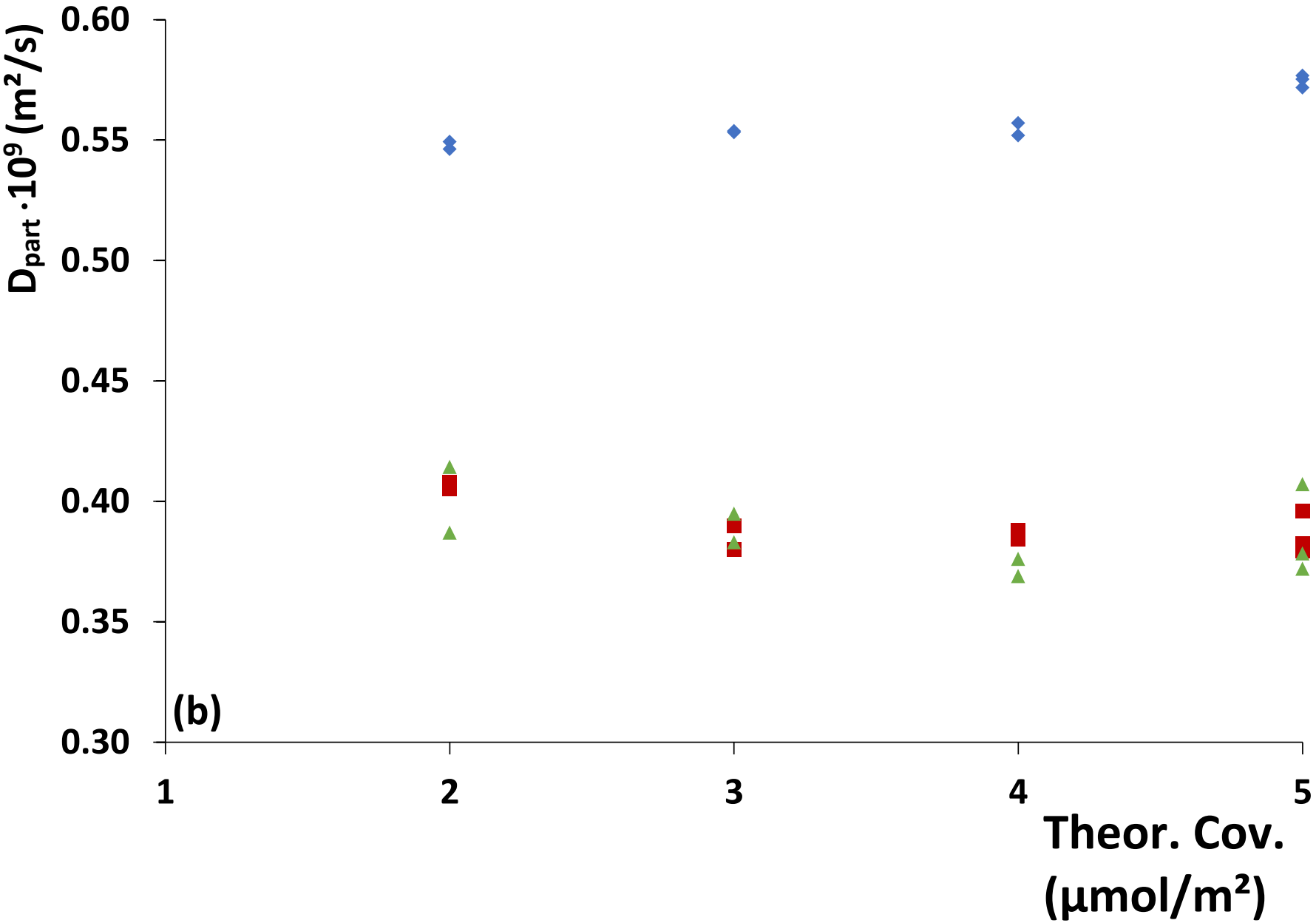
0.60
0.55
0.50
0.45
0.40
0.35
0.30
$D_{part} \cdot 10^9$ (m²/s)
(b)
1
2
3
4
5
Theor. Cov. (µmol/m²)

Figure 5

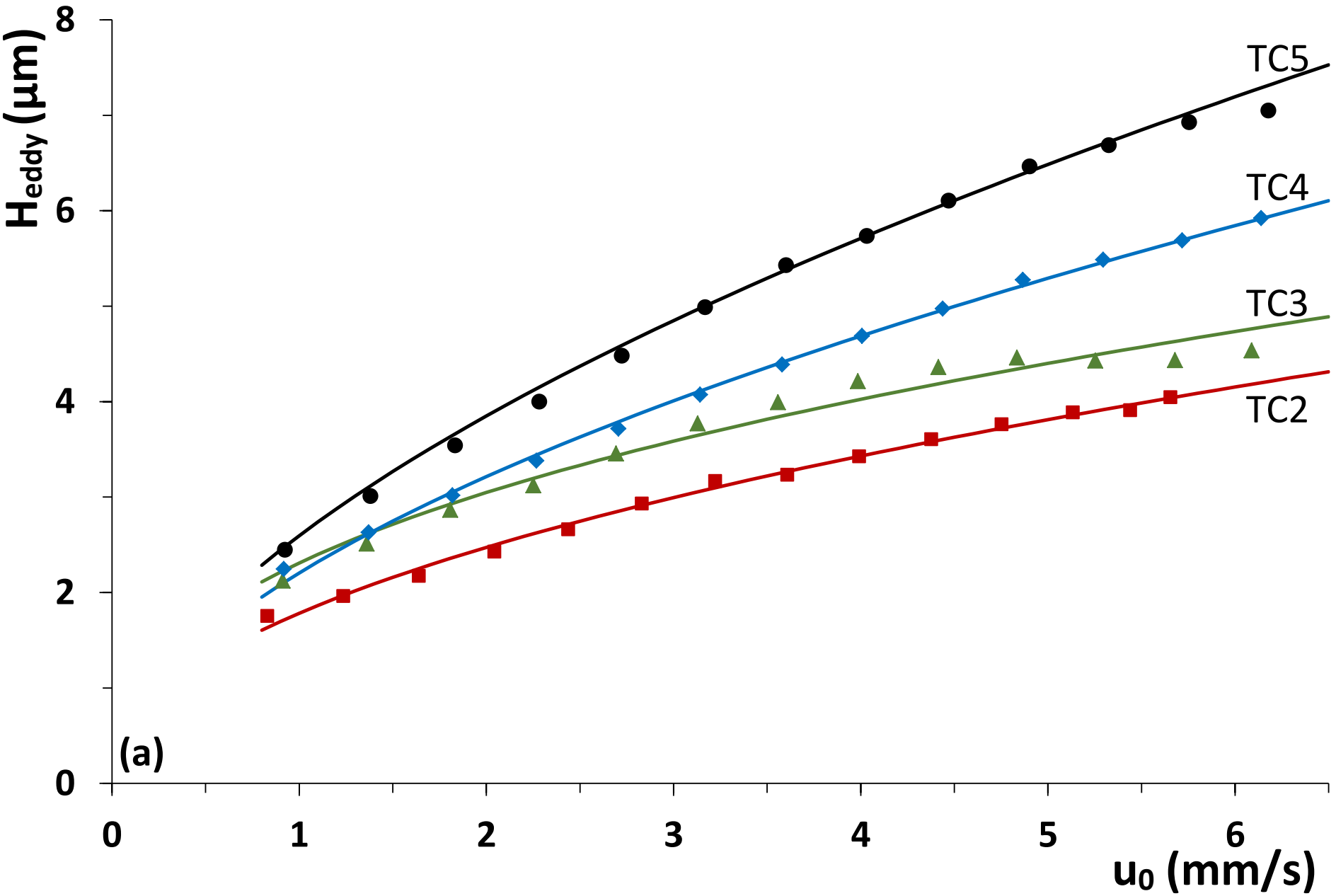

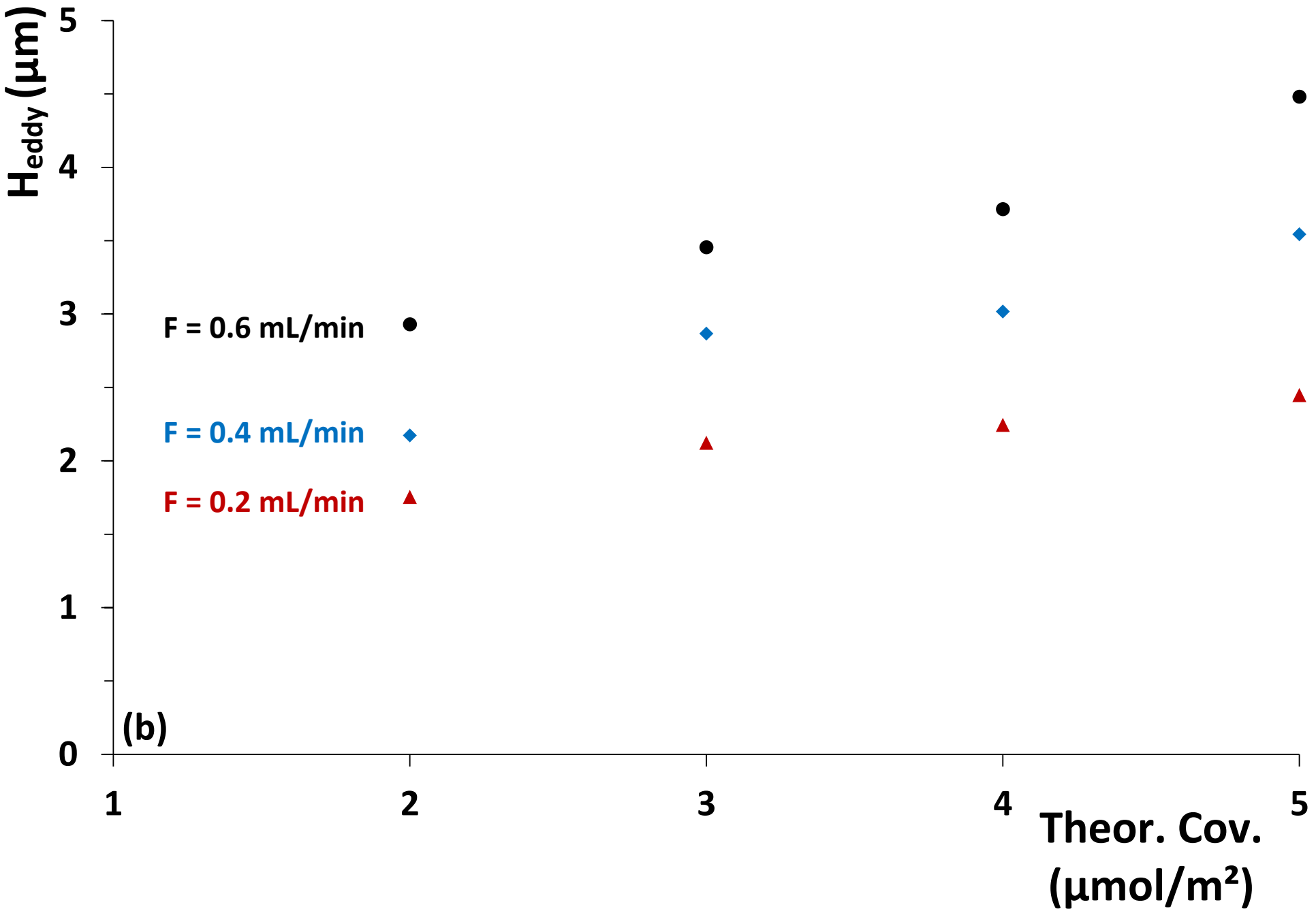
H_{eddy} (µm)
5
4
3
2
1
0
F = 0.6 mL/min
F = 0.4 mL/min
F = 0.2 mL/min
(b)
1
2
3
4
5
Theor. Cov. (µmol/m²)

Figure 6:

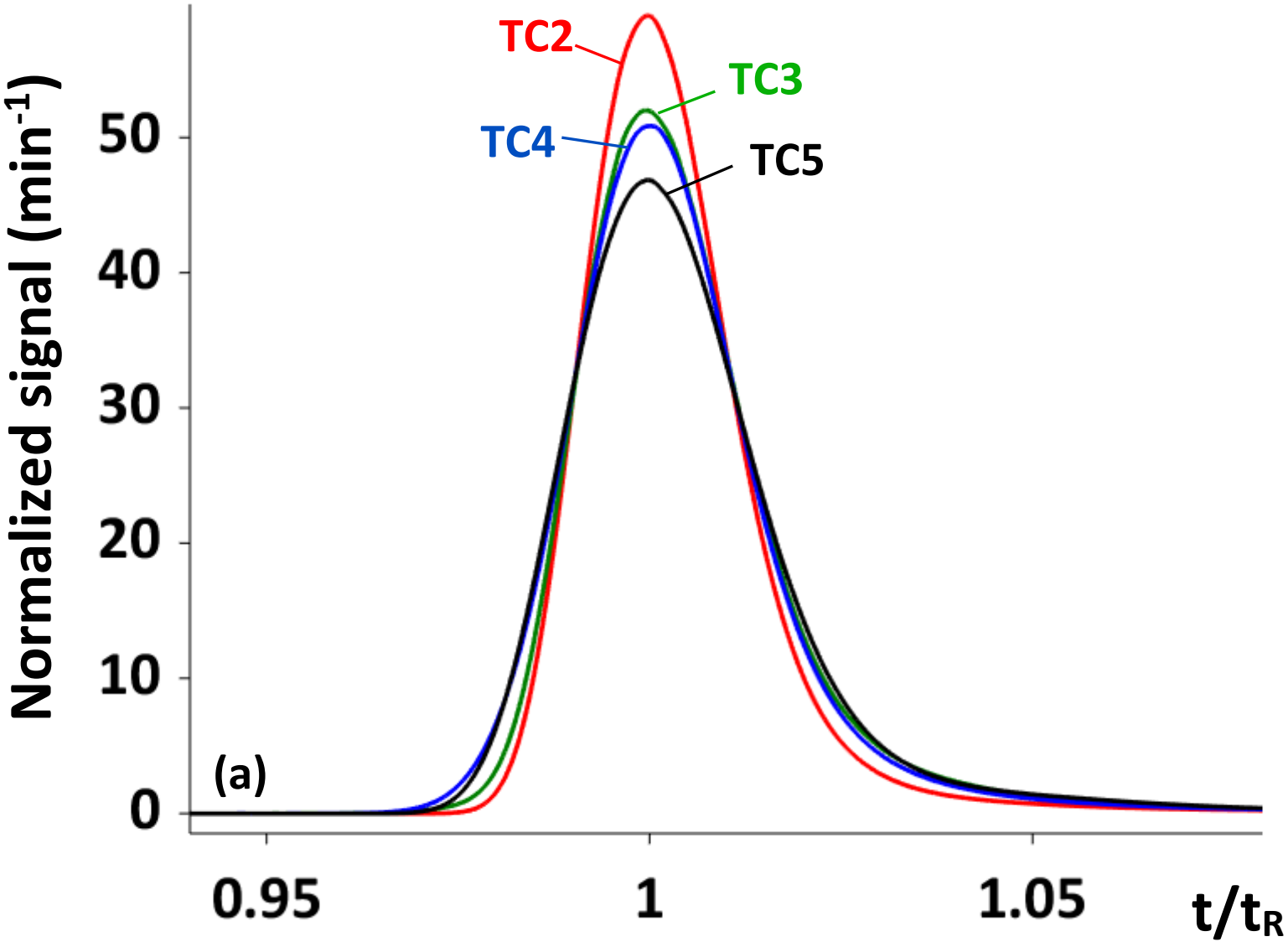
TC2
TC3
TC4
TC5
Normalized signal (min-1)
50
40
30
20
10
0
(a)
0.95
1
1.05
t/tR

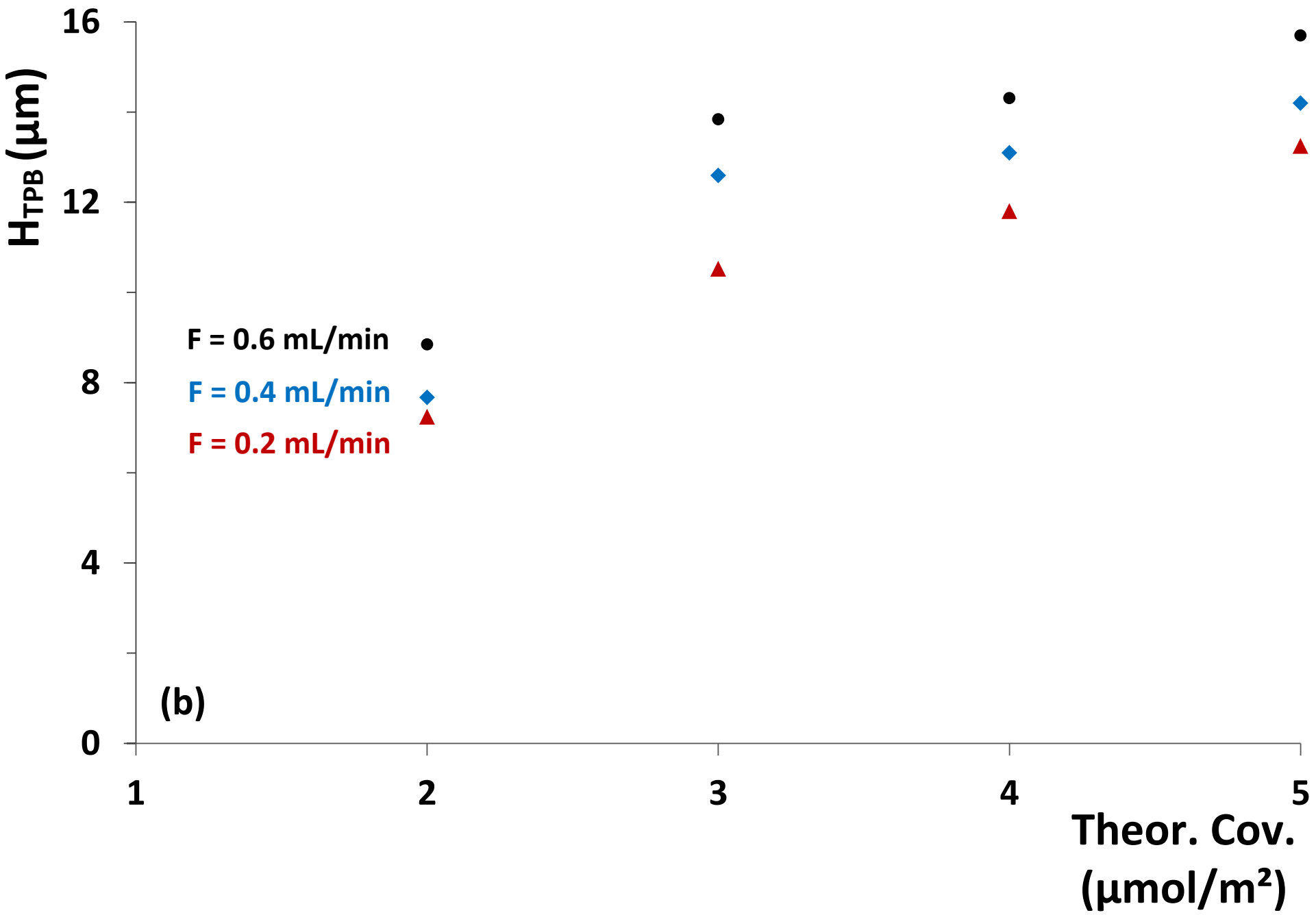
16
12
8
4
0
H_{TPB} (µm)
F = 0.6 mL/min
F = 0.4 mL/min
F = 0.2 mL/min
(b)
1
2
3
4
5
Theor. Cov.
(µmol/m²)

Table 1: *Column properties for the different stationary phases. ε, ε_T and ε_{int} values are the average value of the two tested columns of each phase. The volume fraction of acetonitrile corresponds to the mobile phases used in the van Deemter and peak parking measurements.*

Phase name	Theoretical Coverage µmol/m²	Actual Coverage (Primary) µmol/m²	Actual Coverage (Endcap) µmol/m²	Total Actual Coverage (Prim+Endcap) µmol/m²	External Porosity (TPB), ε in %	Total Porosity (t_0-based) ε_T in %	Internal Porosity ε_{int} in %	V% ACN to obtain k=7 (propioph.)
TC2	2	1.78	1.41	3.19	36.9	54.3	27.5	40.3
TC3	3	2.32	0.97	3.29	37.1	52.9	25.1	39.4
TC4	4	2.53	0.83	3.36	37.1	52.6	24.6	38.4
TC5	5	2.6	0.82	3.42	36.8	52.3	24.5	38.7

Supplementary Material

Effect of Surface Coverage on the Efficiency and Packing Heterogeneity of Packed Bed Columns

Kim Vanderlinden[1], Dave Bell[2], Gert Desmet[1] Ken Broeckhoven[1,]*,

[1] Department of Chemical Engineering, Vrije Universiteit Brussel, Pleinlaan 2, 1050 Brussels, Belgium

[2] MilliporeSigma/Supelco, 595 North Harrison Road, Bellefonte, PA 16823, USA

*Corresponding author: Phone: (+)32.(0)2.629.37.81, Fax: (+)32.(0)2.629.32.48, e-mail: kbroeckh@vub.ac.be

Abstract

In Section 1 of the supplementary materials, retention factor determined in the whole range of conditions (25 to 65 volume% ACN) and the S-values obtained from the fitting of retention factor vs. volumetric fraction of ACN using the LSS-model for the different columns and test compounds are presented. Section 2 shows the result obtained for the individual columns of each tested stationary phase (vs. the averages presented in the main article) and the results for the two other test compounds (less and more retained than propiophenone shown in in the main article). Section 3 gives a brief discussing of the methodology to determine D_{part} and H_{eddy}. Section 4 presents some of the figures from the main articles but plotted vs. the total actual surface coverage rather than the theoretical surface coverage (Fig. 2, 4a and 4b, 5b, 6b).

Section 1:

Fig. S1a shows a plot of ln(k) vs. volume fraction of ACN in the mobile phase measured in the range of 25 to 65% ACN. As can be noted, all applied coating mixtures lead to basically the same ln k versus ϕ-relationship, as all data points relating to the same theoretical C_{18} load basically coincide on the same curve and follow the same slightly non-linear trend with ϕ (coloring in Fig. S1a relates to different components). To guide the eye, average k values were fitted using the Neue-Kuss model [34,35].

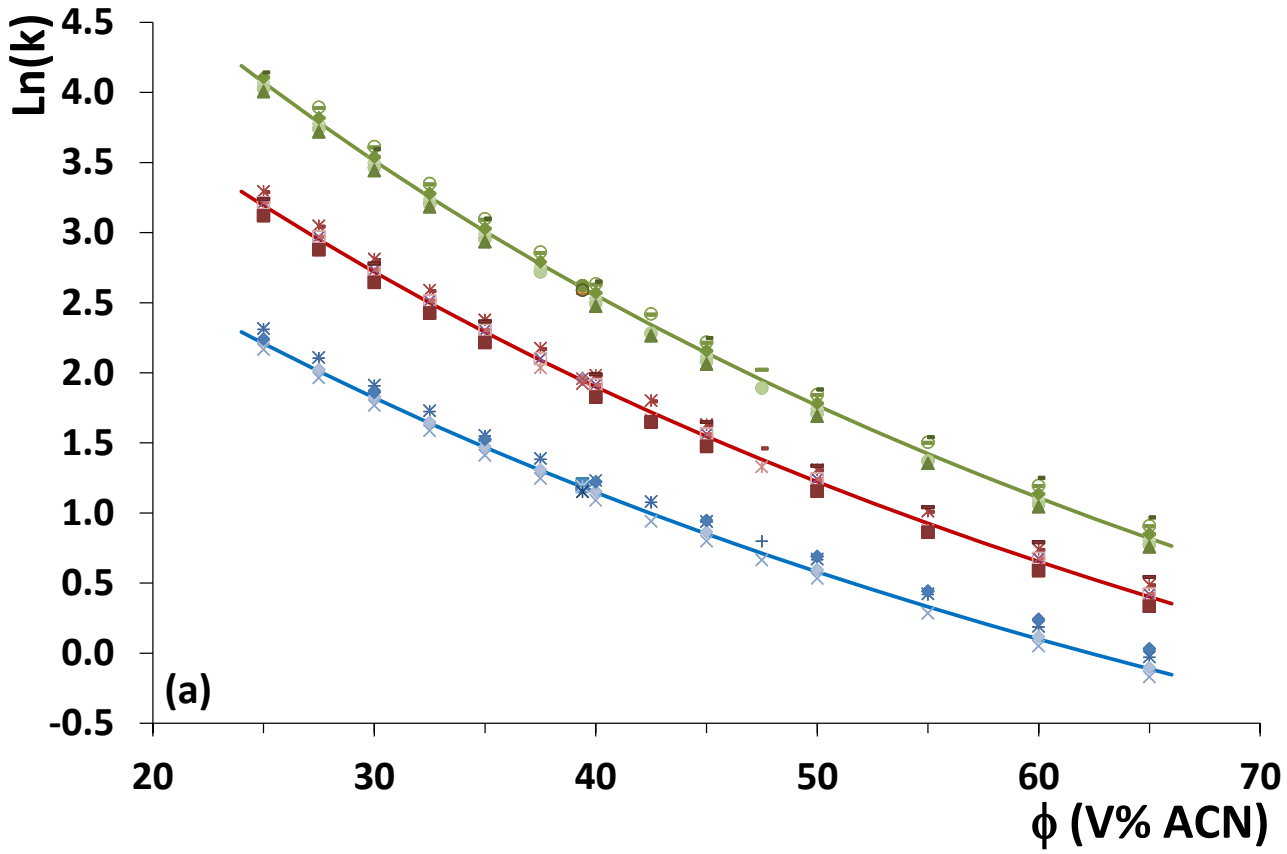

Figure S1a: *Effect of volumetric fraction of acetonitrile in the mobile phase (ACN/H_2O) on the retention factor for acetophenone (blue), propiophenone (red) and butyrophenone (green) for all tested columns (different symbols correspond to the different tested columns), fitted using the Neue-Kuss-model (see Eq. S1) to guide the eye [34,35].*

In Fig. S1a the retention factor was fitted according to the Neue-Kuss model [34,35], which is given by Eq. (S1):

$$k = k_w \cdot (1 + S_2 \cdot \varphi)^2 \cdot e^{-\frac{S_1 \cdot \varphi}{1 + S_2 \cdot \varphi}} \qquad \text{(S1)}$$

For all individual columns, the retention factor was also fitted using the linear solvent strength model to compare the obtained solvent strength parameter S on the different columns using Eq. (S2):

$$k = k_w \cdot e^{-S \cdot \varphi} \qquad \text{(S2)}$$

The obtained S values vs. theoretical surface coverage are plotted in Fig. S1b, showing little to no variation in S with theoretical C_{18} coverage.

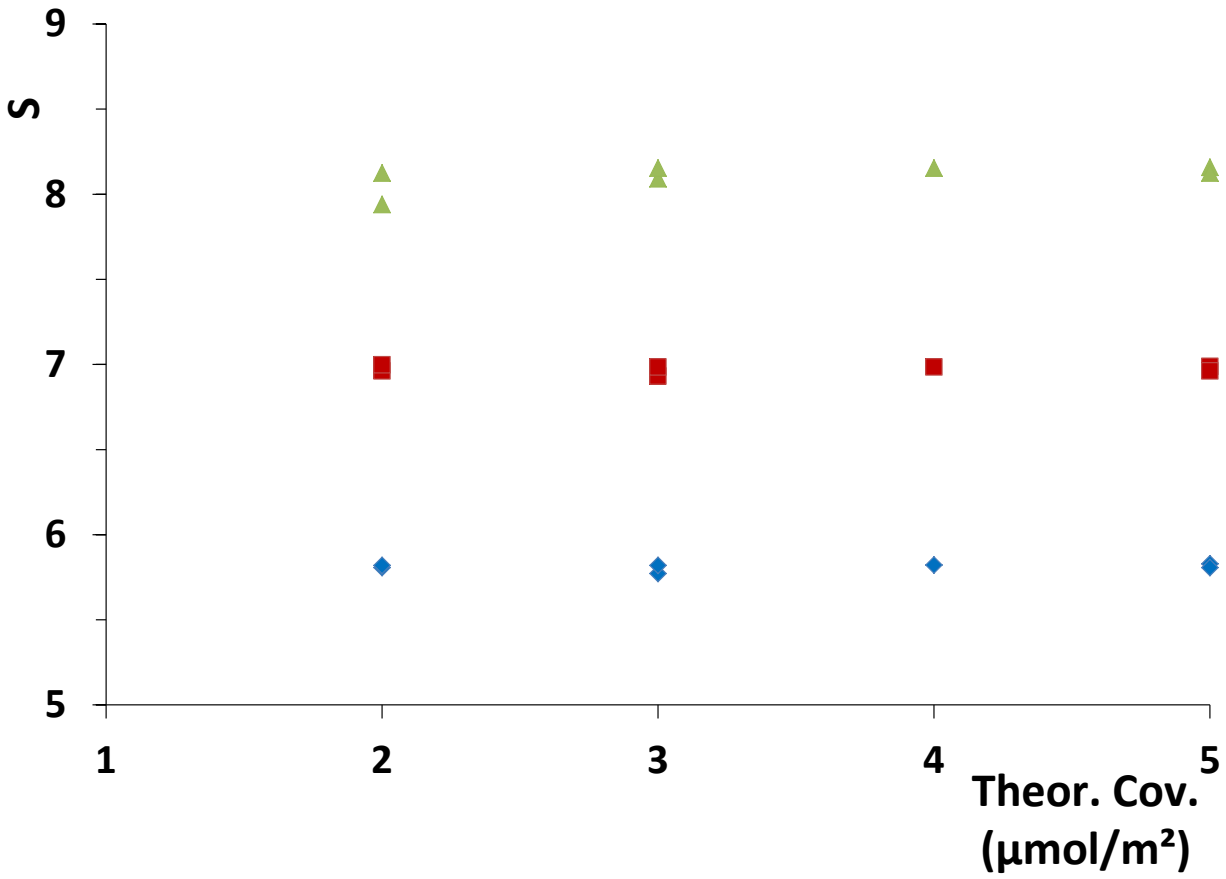

Figure S1b: *Plot of the linear solvent strength factor S for the different theoretical C_{18} coverages; symbols: acetophenone (diamonds), propiophenone (squares) and butyrophenone (triangles).*

Section 2:

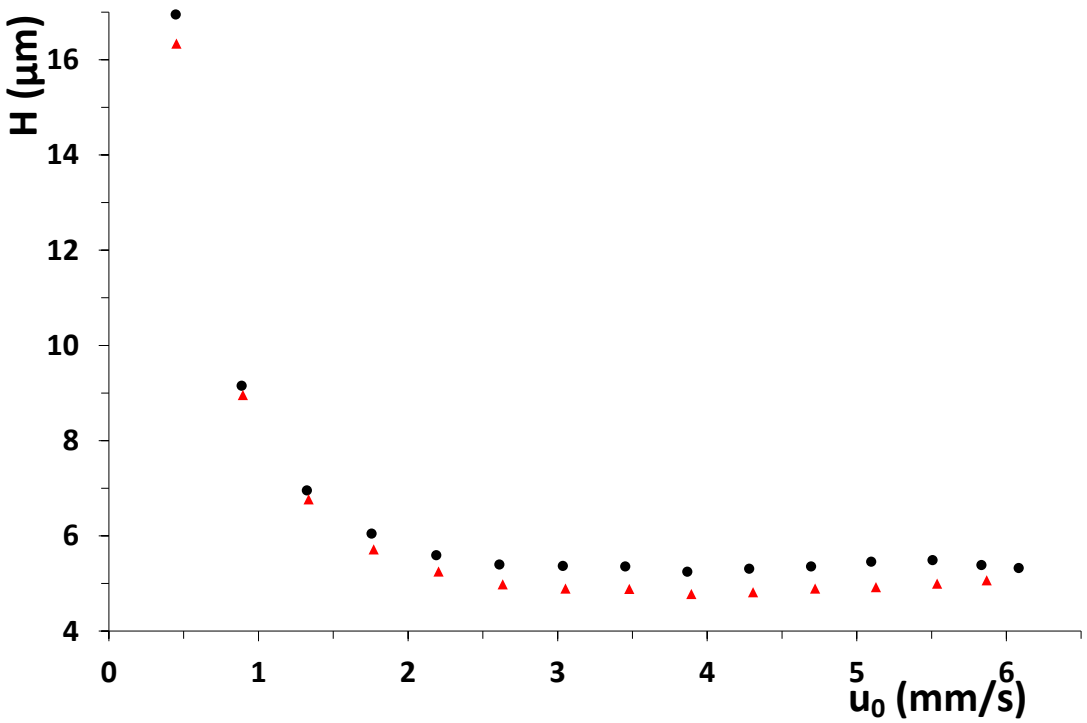

Figure S2a: *Plot of plate height vs. linear velocity for the individual columns packed with same stationary phase (**TC2**) and propiophenone as sample compound: TC-1 (circles), TC-2 (triangles).*

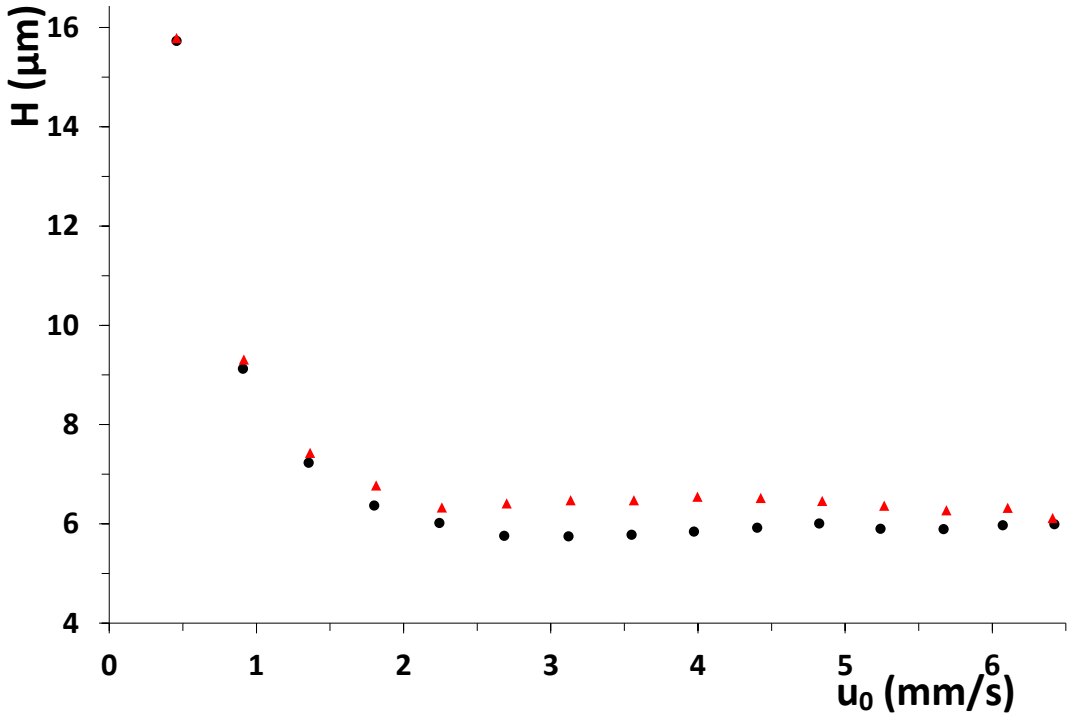

Figure S2b: *Plot of plate height vs. linear velocity for the individual columns packed with same stationary phase (**TC3**) and propiophenone as sample compound: TC-1 (circles), TC-2 (triangles).*

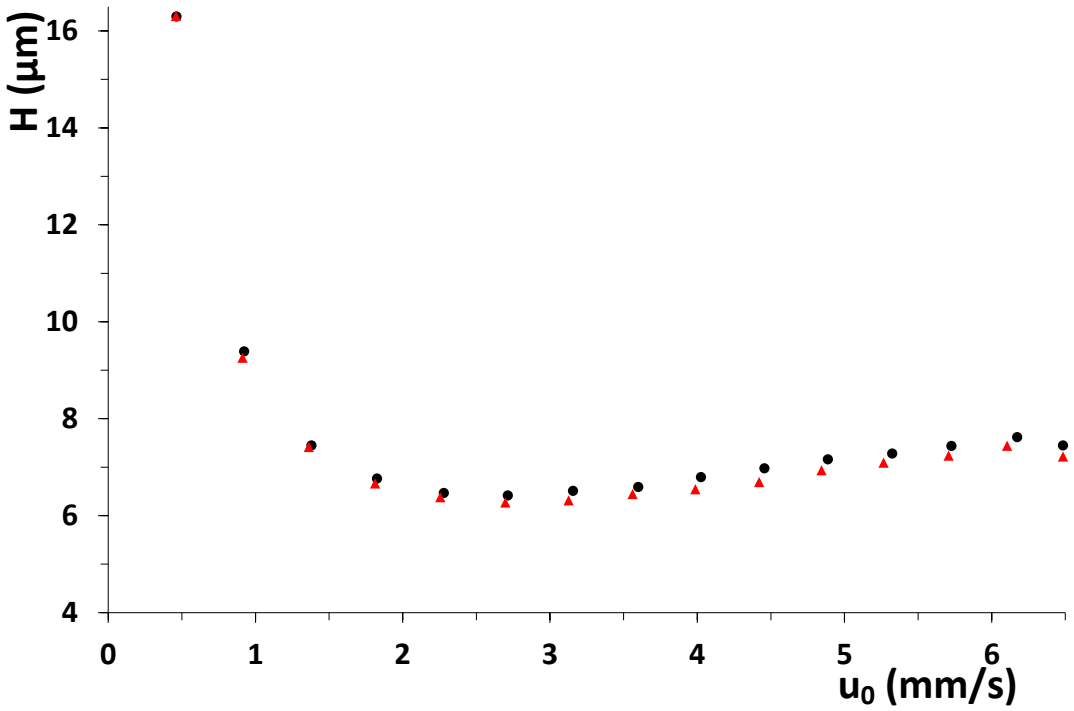

Figure S2c: *Plot of plate height vs. linear velocity for the individual columns packed with same stationary phase (**TC4**) and propiophenone as sample compound: TC-1 (circles), TC-2 (triangles).*

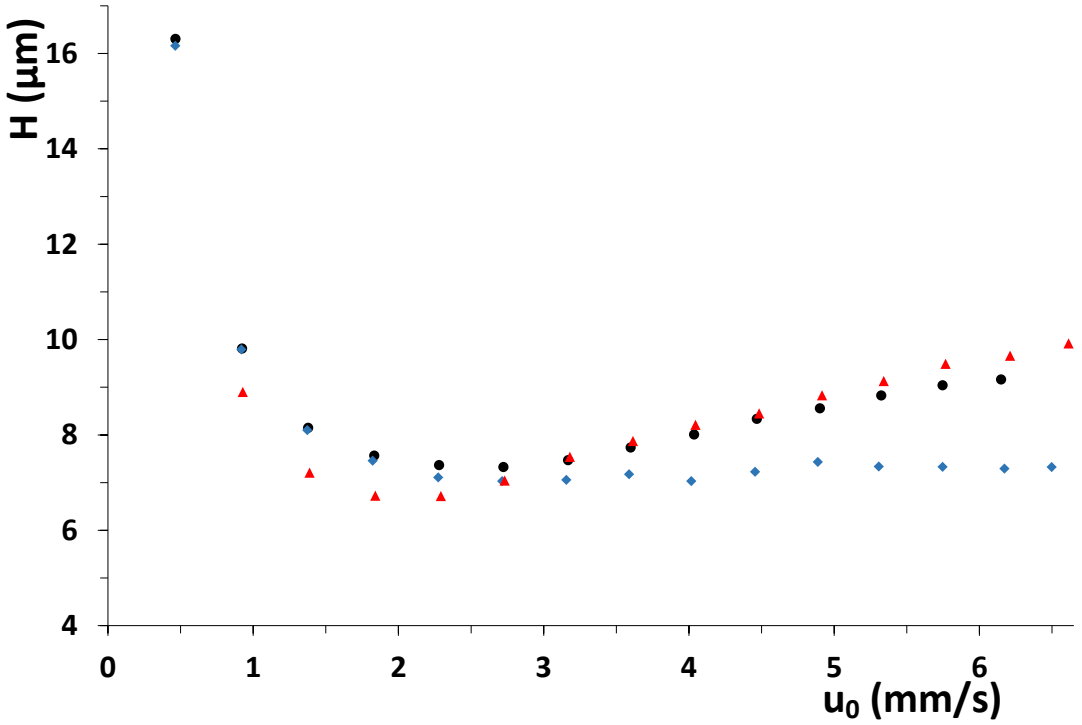

Figure S2d: *Plot of plate height vs. linear velocity for the individual columns packed with same stationary phase (**TC5**) and propiophenone as sample compound: TC-1 (circles), TC-2 (triangles), TC-3 (diamonds).*

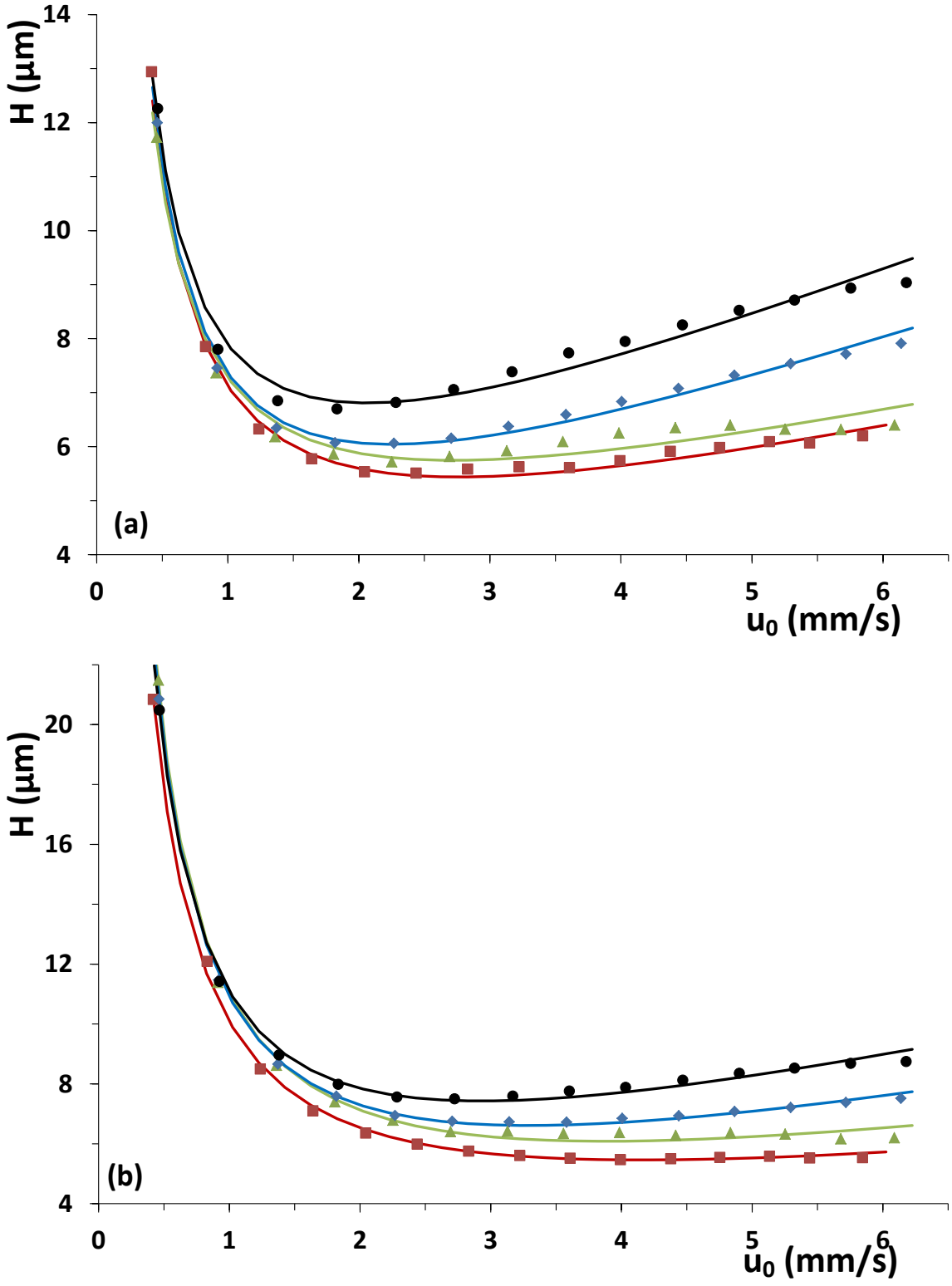

Figure S3: *Plot of plate height vs. linear velocity for the different theoretical surface coverages for* ***(a)*** *acetophenone and* ***(b)*** *butyrophenone; each data set presents the average of two columns with the same stationary phase (or three for TC5). Fit curves according to the van Deemter equation to guide the eye. Symbols: TC2 (squares), TC3 (triangles), TC4 (diamonds), TC5 (circles).*

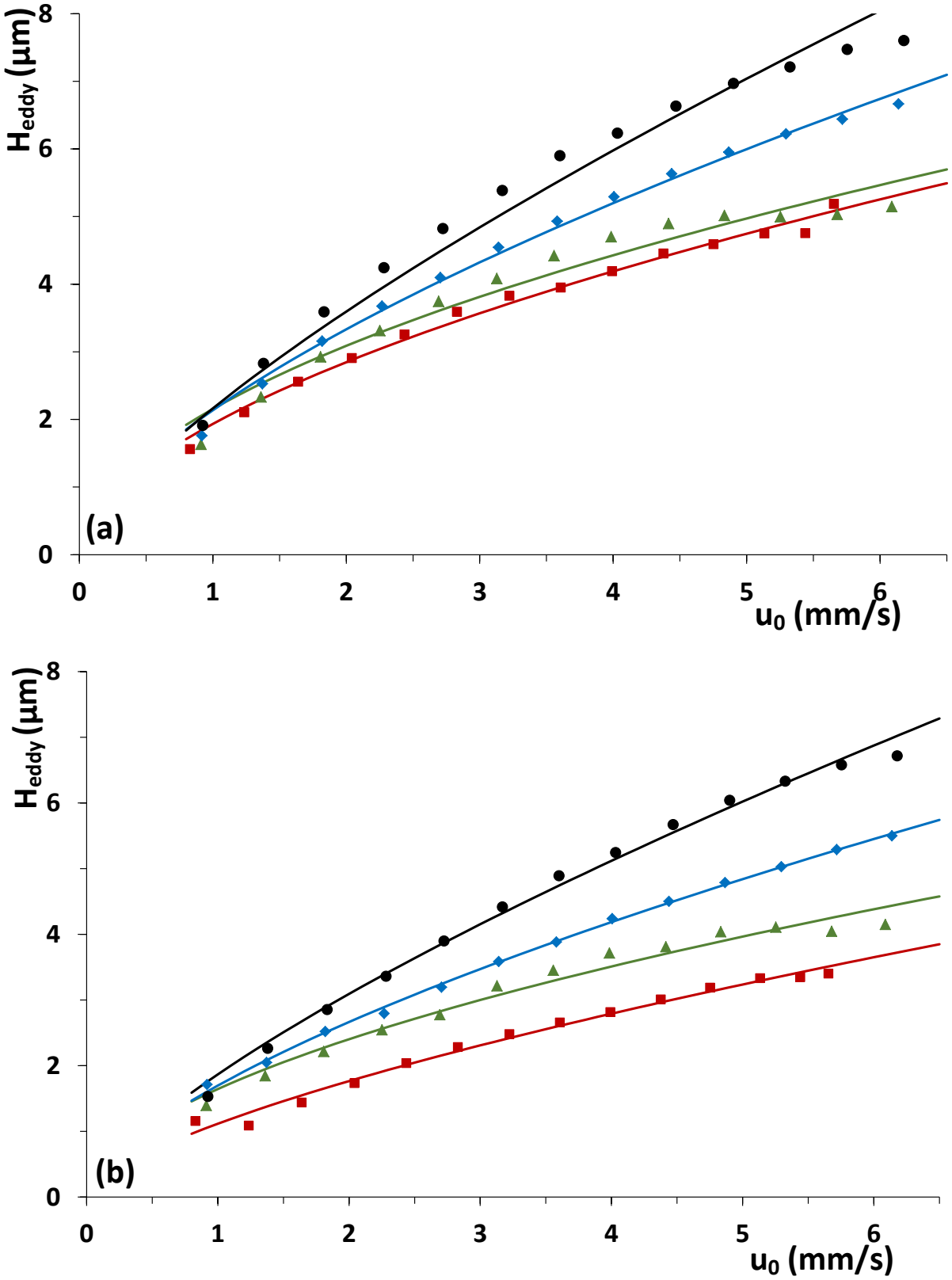

Figure S4: *Plot of the eddy dispersion contribution vs. velocity to the overall H for the different surface coverages, fit curves to guide the eye,* ***(a)*** *acetophenone and* ***(b)*** *butyrophenone as sample compound.*

Section 3:

To determine the value for D_{part}, the experimentally determined values of D_{eff}, combined with the values of the sample diffusion coefficient D_m, the external (ε) and total porosity (ε_T), are used to calculate the polarizability constant β_1 and relative permeability of spherical particles $\alpha_{part,}$ that, in the case of packed bed column, are given by:

$$\beta_1 = \frac{1}{1-\varepsilon}\frac{\frac{D_{eff}}{D_m}\cdot\varepsilon_T(1+k')-1}{2+\frac{D_{eff}}{D_m}\cdot\varepsilon_T(1+k')} \quad \text{and} \quad \alpha_{part} = \frac{1+2\beta_1}{1-\beta_1} \tag{S3}$$

Using the Maxwell EMT model, the diffusion inside the particle D_{part} can be obtained by means of the expression [44]:

$$D_{part} = \frac{\alpha_{part}\cdot(1-\varepsilon_e)}{\varepsilon_T\cdot(1+k')-\varepsilon_e}D_m \tag{S4}$$

Since fully porous particle are used in this work, the value of D_{part} is the same as that of the porous zone D_{pz} (for the case of superficially porous particles this no longer holds) and this allows to calculate the stationary phase mass transfer contribution to H as [38,46]:

$$H_{C_s} = \frac{2}{\alpha}\frac{1}{Sh_{part}}\frac{k''}{(1+k'')^2}u_i\frac{d_p^{\,2}}{D_{part}} \tag{S5}$$

Where α is a coefficient that takes the value of 6 for spherical particles, k'' is the zone retention factor ($k''=(1+k)\cdot\varepsilon_T/\varepsilon-1$ for fully porous particles), u_i is the interstitial velocity of the mobile phase ($u_i=u_0\cdot\varepsilon/\varepsilon_T$) and d_p is the particle size. Sh_{part} stands for the Sherwood number of the stationary phase particles which in the case of fully porous particles is equal to 10. The mobile phase mass transfer contribution to H is calculated using [46]:

$$H_{C_m} = 2\frac{k''^2}{(1+k'')^2}\frac{\nu_i}{\alpha}\frac{1}{Sh_m}\frac{\varepsilon}{1-\varepsilon} \tag{S6}$$

Using the expression for Sh_m derived in [47] for $0.35<\varepsilon<0.44$ and for the reduced interstitial velocities ν_i ($\nu_i=u_i\cdot d_p/D_m$) in the range $1<\nu_i<250$:

$$Sh_m = \frac{13}{(1+2.1\cdot\nu_i)}+8.6\cdot\nu_i^{\,0.21} \tag{S7}$$

The H_{eddy} contribution is then calculated based on the experimental H values by:

$$H_{eddy} = H-H_{C_m}-H_{C_s}-H_B \quad \text{with} \quad H_B = 2\cdot\frac{D_{eff}}{u_0}\cdot(1+k) \tag{S8}$$

A template for this calculation can be downloaded using the following link [38]:
http://vubchemicalengineering.be/wp-content/uploads/2018/02/Detailed-column-performance-analyzer_19-02-2018.xlsx

Section 4:

Figures 2, 4a and 4b, 5b, 6b from the main articles but plotted vs. the total actual surface coverage rather than the theoretical surface coverage.

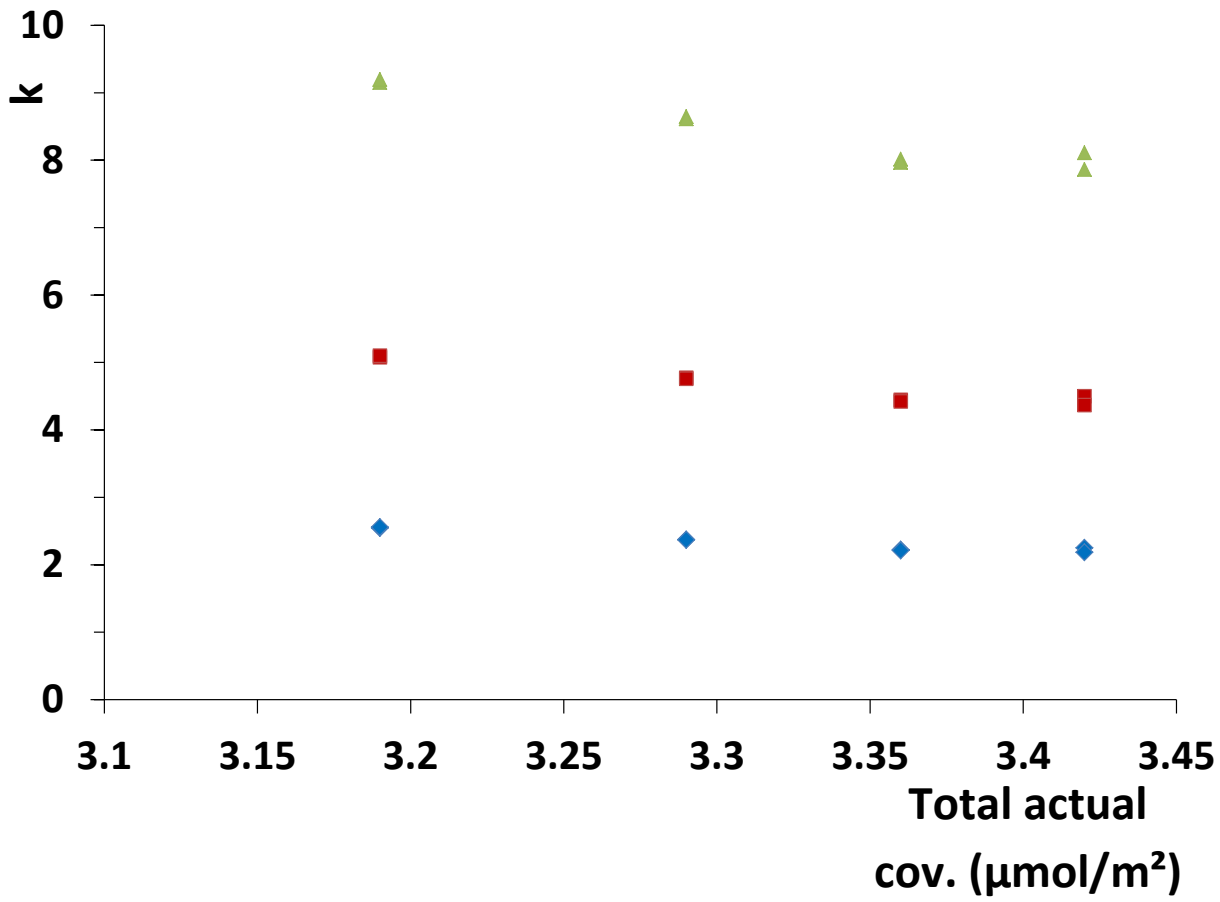

Figure S5: *Same figure as Fig. 2 in the main article, but plotted vs. total actual surface coverage rather than the theoretical surface coverage.*

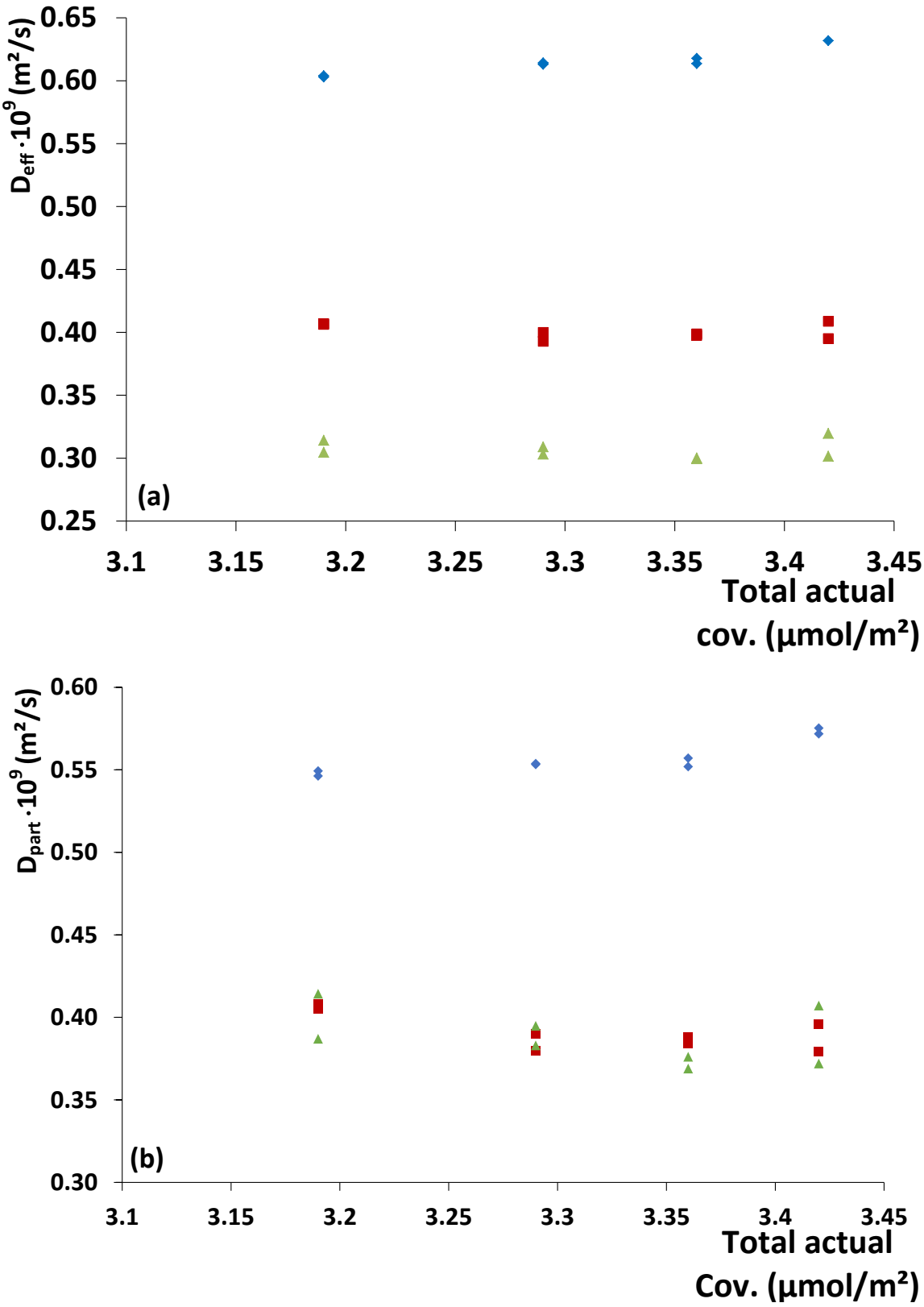

Figure S6: *Same figure as Fig. 4 in the main article, but plotted vs. total actual surface coverage rather than the theoretical surface coverage.*

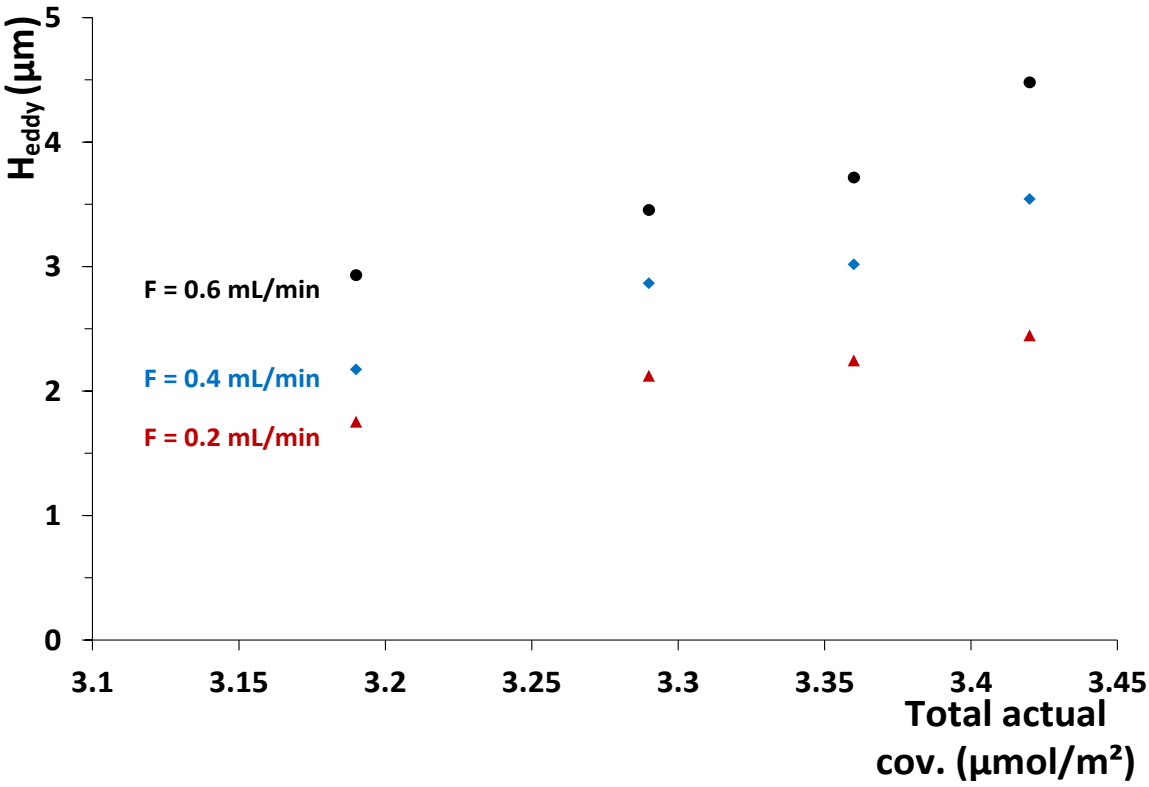

Figure S7: *Same figure as Fig. 5b in the main article, but plotted vs. total actual surface coverage rather than the theoretical surface coverage.*

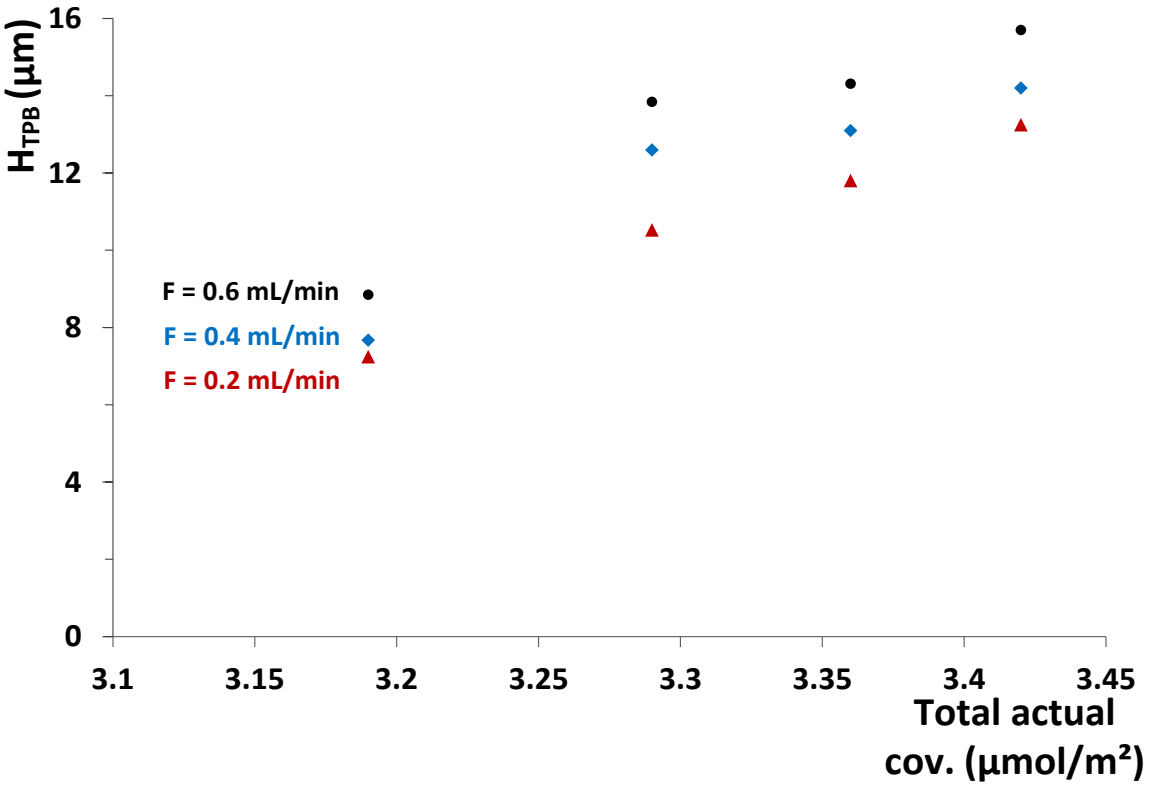

Figure S8: *Same figure as Fig. 5b in the main article, but plotted vs. total actual surface coverage rather than the theoretical surface coverage.*